Journal of Medicinal Chemistry

Article

pubs.acs.org/jmc

Discovery of Oral VEGFR-2 Inhibitors with Prolonged Ocular Retention That Are Efficacious in Models of Wet Age-Related Macular Degeneration

Erik L. Meredith,[*,†] Nello Mainolfi,[†,⊥] Stephen Poor,[‡] Yubin Qiu,[‡] Karl Miranda,[†,▽] James Powers,[†] Donglei Liu,[†] Fupeng Ma,[†] Catherine Solovay,[†] Chang Rao,[†,∞] Leland Johnson,[†,○] Nan Ji,[†,◆] Gerald Artman,[†,¶] Leo Hardegger,[†,+] Shawn Hanks,[‡] Siyuan Shen,[‡] Amber Woolfenden,[‡] Elizabeth Fassbender,[‡] Jeremy M. Sivak,[‡,#] Yiqin Zhang,[‡,÷] Debby Long,[‡] Rosemarie Cepeda,[‡] Fang Liu,[‡] Vinayak P. Hosagrahara,[§,×] Wendy Lee,[§] Peter Tarsa,[∥] Karen Anderson,[‡] Jason Elliott,[†] and Bruce Jaffee[‡]

[†]Global Discovery Chemistry, Novartis Institutes for BioMedical Research, 100 Technology Square, Cambridge, Massachusetts 02139, United States

[‡]Ophthalmology, Novartis Institutes for BioMedical Research, 500 Technology Square, Cambridge, Massachusetts 02139, United States

[§]Metabolism and Pharmacokinetics, Novartis Institutes for BioMedical Research, 250 Massachusetts Avenue, Cambridge Massachusetts 02139, United States

[∥]Chemical and Pharmaceutical Profiling, Novartis Institutes for BioMedical Research, 500 Technology Square, Cambridge, Massachusetts 02139, United States

ABSTRACT: The benefit of intravitreal anti-VEGF therapy in treating wet age-related macular degeneration (AMD) is well established. Identification of VEGFR-2 inhibitors with optimal ADME properties for an ocular indication provides opportunities for dosing routes beyond intravitreal injection. We employed a high−throughput *in vivo* screening strategy with rodent models of choroidal neovascularization and iterative compound design to identify VEGFR-2 inhibitors with potential to benefit wet AMD patients. These compounds demonstrate preferential ocular tissue distribution and efficacy after oral administration while minimizing systemic exposure.

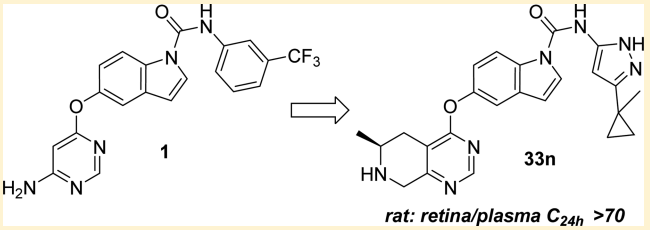

INTRODUCTION

Age-related macular degeneration (AMD) is an eye disease that causes vision loss due to pathology in the macula, the area of the retina that enables sharp and detailed vision. AMD is responsible for the majority of cases of blindness and visual impairment in aged adults. In the wet form of AMD, choroidal blood vessels (choroidal neovascularization, CNV) sprout and expand into the submacular space leaking fluid and blood. This leads to retinal edema, scar tissue formation, and irreversible damage to the macula. The current approved therapies for wet AMD are the anti-VEGF-A antibody ranibizumab, the anti-VEGF-A aptamer pegaptanib, and the anti-VEGF-A and PLGF fusion protein aflibercept. All are delivered by intravitreal injection (i.v.t.), a procedure that carries a small, but significant, risk of blinding complications including endophthalmitis, retinal detachment, or uveitis. Ranibizumab and aflibercept are the most effective, stabilizing vision in 60% patients and significantly improving vision (gain of 3 lines of vision on an ETDRS reading chart) in approximately 1/3 of patients.[1] Injections are administered monthly or bimonthly, which is a significant burden for patients and retinal doctors. Even with anti-VEGF therapy, wet AMD patients still have substantial visual deficit.[2] We envisioned an opportunity for a less invasive wet AMD therapy based on an orally available inhibitor of the receptor tyrosine kinase (RTK) VEGFR-2 (KDR, Flt-1). An oral therapy may provide greater efficacy than intravitreal therapy by enabling more frequent dosing and greater target tissue exposure.

The role of VEGF-A in the regulation of angiogenesis is well established. Although new vessel growth and maturation are highly complex processes, requiring the sequential activation of a series of receptors by numerous ligands, VEGF-A signaling is a critical rate-limiting step.[3] VEGF-A promotes growth of vascular endothelial cells and is also known to induce vascular leakage.[4] Ocular VEGF-A levels are increased in preclinical models and human diseases of ocular angiogenesis including wet AMD,[5,6] diabetic retinopathy, and retinal vein occlusions.[7,8]

VEGF-A binds to two related receptor tyrosine kinases, VEGFR-1 and VEGFR-2, which both have an extracellular domain consisting of 7 immunoglobulin-like domains, a single transmembrane region, and a consensus tyrosine kinase

Received: August 3, 2015
Published: November 15, 2015

DOI: 10.1021/acs.jmedchem.5b01227
J. Med. Chem. 2015, 58, 9273−9286

Table 1. *In Vitro* Inhibition Data (KDR Biochemical; BaF3 Cellular) and *in Vivo* (% Inhibition of Mouse CNV) for Selected Compounds

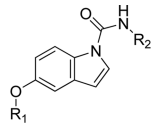

CMPD	R_1	R_2	KDR IC_{50} (nM)[a]	BaF3 IC_{50} (nM)[a]	mCNV % inhibition @ 10 mg/kg qd[b]
1	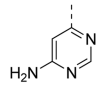		17	--	44
5a	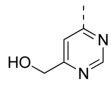		13	4	45
6a	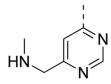		8	11	67
6b	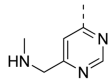		5	66	92
33a	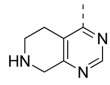		22	10	87
33b	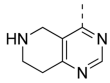		18	81	0
33c	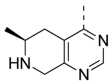		24	60	96
33d	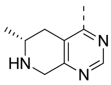		23	109	58
33e	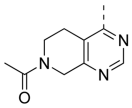		7	--	0
33f	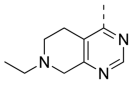		10	10	81
33g	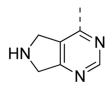		29	0.4	68
33h	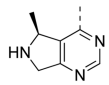		16	118	41
33i	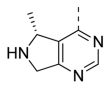		17	--	0
33j	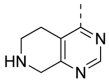		280	1922	--
33k	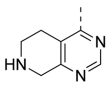		6	3	0
33l	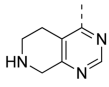	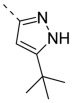	8	1	0
33m	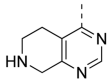	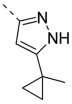	5	3	64
33n	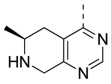	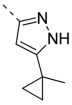	8	0.9	67
33o	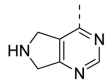	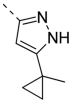	< 3	0.5	43
33p	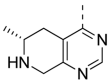		8	0.9	48
33q			30	40	83
33r			30	4	96
33s			9	59	83
33t			114	167	58
33u			22	8	33
33v			41	26	98
33w			9	2	96
33x			14	6	90

[a]Values are the mean of at least two experiments (IC_{50}, nM). [b]Compounds dosed q.d. orally as 0.5% CMC/0.1% Tween 80.

sequence that is interrupted by a kinase-insert domain.[9] VEGFR-2 (KDR or Flt-1) is implicated in all aspects of normal and pathological vascular endothelial cell biology. VEGFR-2 is the major mediator of the mitogenic, angiogenic,

DOI: 10.1021/acs.jmedchem.5b01227
J. Med. Chem. 2015, 58, 9273−9286

Scheme 1[a]

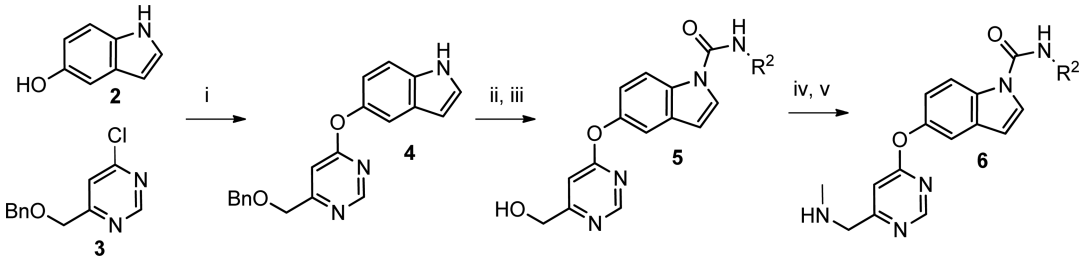

[a]Reagents and conditions: (i) DBU, CH_3CN, 75%; (ii) NaH, R^2NCO, DMF, −50 °C to rt, 88%; (iii) TFA, 100 °C, 74%; (iv) Ms_2O, pyridine, THF; (v) CH_3NH_2, MeOH, 54%, 2 steps.

Scheme 2[a]

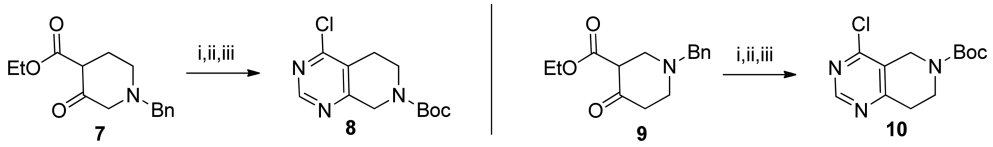

[a]Reagents and conditions: (i) formamidine acetate, EtONa, EtOH, reflux, 90%; (ii) Pd/C, Boc_2O, MeOH/THF; (iii) CCl_4, PPh_3, DCE, reflux, 80%, 2 steps.

Scheme 3[a]

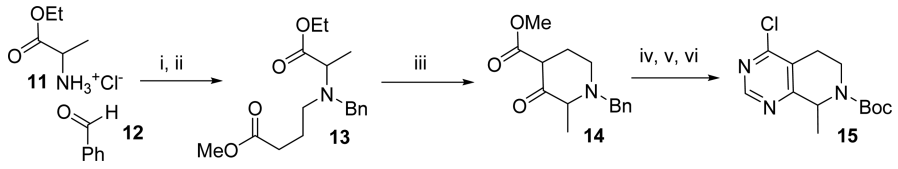

[a]Reagents and conditions: (i) **11**, **12**, $NaBH(OAc)_3$, TEA, DCE; (ii) ethyl oxobutanoate, $NaBH(OAc)_3$, DCE; (iii) *t*BuOK, toluene; (iv) formamidine acetate, EtONa, EtOH, reflux, 36% 4 steps; (v) Pd/C, Boc_2O, MeOH; (vi) CCl_4, PPh_3, DCE, reflux 57%, 2 steps.

and permeability-enhancing effects of VEGF-A. VEGFR-2 null mice die *in utero* between days 8.5−9.5 and are characterized by a lack of vasculogenesis and failure to develop organized blood vessels.[10] Upon VEGF-A binding, VEGFR-2 undergoes dimerization and ligand-dependent tyrosine phosphorylation in intact cells, resulting in a mitogenic, chemotactic, and survival signal.[11]

Systemic inhibition of the VEGF pathway is known to cause on-target side effects including hypertension, proteinuria, bleeding, thromboembolism, and gastrointestinal perforation.[12] Our strategy to mitigate the risk of systemic VEGF inhibition was to identify compounds with preferential distribution and retention in ocular tissues (retina and retinal pigment epithelium/choroid) compared to the plasma.

There are a number of approved orally administered VEGFR-2 inhibitors for oncology indications and several have been investigated in wet AMD.[13−15] In a published case study, treatment with oral sorafenib correlated with reduced retinal edema and increased visual acuity.[16,17] More recently, orally dosed pazopanib is reported to improve vision, reduce edema, and reduce neovascularization in wet AMD patients.[18] Despite the fact the doses used were markedly less than those in oncology indications, systemic side effects were still observed. Thus, a compound that more selectively targets ocular tissues than marketed oncology drugs would potentially be an effective and safer therapy for wet AMD patients.

To achieve our objective of identifying compounds with preferential ocular distribution, we understood that relatively high-throughput *in vivo* models of ocular angiogenesis would be needed to establish both ocular efficacy and tissue distribution relationships. The primary *in vivo* models utilized were laser-induced choroidal neovascularization (CNV) in mice and in rats. Briefly, photocoagulating green laser pulses are applied to the eye in order to cause a focal rupture of Bruch's membrane, an extracellular matrix between the retina and choroid. Rupture of Bruch's membrane induces production of local inflammatory factors and VEGF resulting in choroidal neovascularization (CNV). CNV formation in response to laser injury has been demonstrated in humans, monkeys, pigs, and rodents and is a VEGF-dependent pathology.[19]

Evaluation of several internal VEGFR-2 kinase inhibitors in the mouse CNV model provided **1**[20] (Table 1) as a promising starting point for chemistry optimization. The compound demonstrated a modest level of inhibition (44%) but had poor aqueous solubility (<5 μM at pH 6.8). Thus, we undertook a strategy to identify compounds with greater efficacy and improved ADME properties.

Chemistry. The preparation of monocyclic pyrimidine analogues such as **6** was carried out as described in Scheme 1. Coupling of indole **2** with pyrimidine **3**[21] was achieved by treatment with DBU. Formation of the urea was then accomplished by trapping the lithium anion of the indole with the desired phenylisocyanates. Removal of the benzyl protecting group with TFA provided alcohol **5**, which was readily converted to methylamine **6** by conversion first to the mesylate and then displacement with methylamine.

The bicyclic pyrimidine intermediates **8** and **10** were accessible from the corresponding β-ketoesters **7** and **9**,

DOI: 10.1021/acs.jmedchem.5b01227
J. Med. Chem. 2015, 58, 9273−9286

Scheme 4[a]

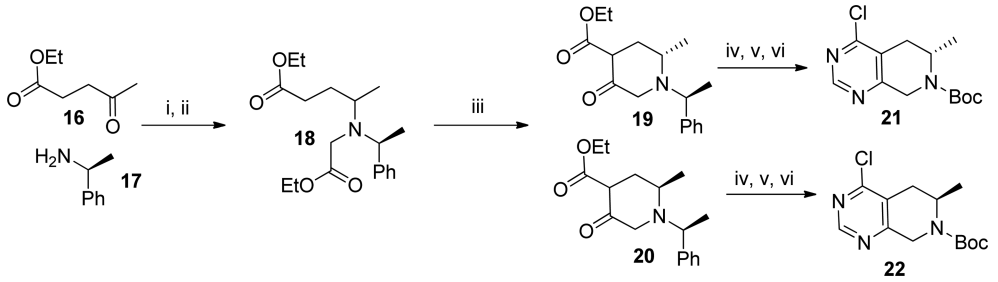

[a]Reagents and conditions: (i) **16**, **17**, $NaBH(OAc)_3$, DCE; (ii) ethyl glyoxylate, $NaBH(OAc)_3$, DCE; (iii) *t*BuOK, toluene, 50−70%, 3 steps; (iv) formamidine acetate, EtONa, EtOH, reflux, 93%; (v) Pd/C, Boc_2O, EtOH, 80%, 2 steps; (vi) CCl_4, PPh_3, DCE, reflux, 51%.

respectively (Scheme 2). Treatment of each *β*-ketoester **7** and **9** with formamidine acetate provided the corresponding hydroxypyrimidine, which then underwent a protecting group swap from benzyl to Boc. Conversion to the chloropyrimidines **8** and **10** was then accomplished by reaction with carbon tetrachloride and triphenylphosphine.

The 8-methyl substituted bicyclic pyrimidine **15** was prepared as outlined in Scheme 3. The *β*-ketoester **14** was converted to the corresponding Boc protected chloropyrimidine by analogy to that of **8** and **10**.

The chiral chloropyrimidines **21** and **22** were prepared starting from (*S*)-*α*-methylbenzylamine, which underwent reductive amination with **16** and then ethyl glyoxylate to provide diester **18** (Scheme 4). Claisen condensation of **18** then provided diastereomers **19** and **20**, which were separated by flash chromatography. Conversion of each diastereomer **19** and **20** to the corresponding chloropyrimidines **21** and **22** was achieved under the same conditions as those described above.

The 6,5-bicyclic pyrimidine **24** was prepared by condensation of the commercially available *β*-ketoester **23** with formamidine acetate (Scheme 5). Construction of the methyl

Scheme 5[a]

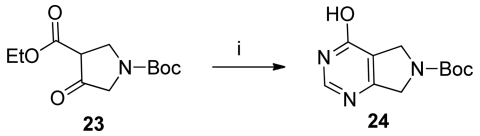

[a]Reagents and conditions: (i) formamidine acetate, EtONa, EtOH, reflux, 24%.

substituted 6,5-bicyclic pyrimidine was as described in Scheme 6. In each of these cases, the hydroxy pyrimidines were used in the subsequent coupling steps as the chloro derivatives were found to be both difficult to prepare and use due to instability.

Coupling of the bicyclic pyrimidines **10**, **15**, **21**, and **22** to the hydroxyindole was achieved by treatment with DBU to give the corresponding derivatives **30** (Scheme 7). The 6,5-bicyclic

Scheme 7[a]

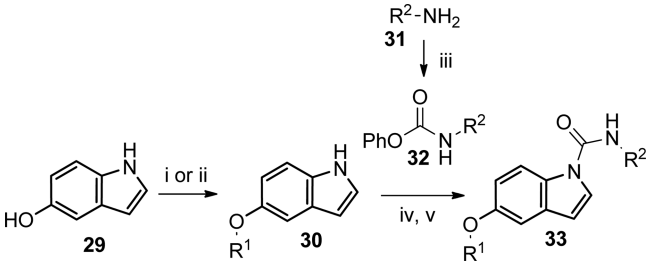

[a]Reagents and conditions: (i) **10**, **15**, **21**, or **22**, DBU, CH_3CN, reflux, 90%; (ii) **24** or **28**, PyBop, acetonitrile, DBU, 64%; (iii) **25**, phenyl chloroformate, pyridine, 86%; (iv) **32** or R^2NCO, NaH, THF, 0 °C-rt, 50%; (v) TFA, DCM, 92%.

pyrimidines **24** and **28** were efficiently coupled to **29** with PyBop and DBU.[22] Formation of the desired urea analogues **33** was achieved by treatment of the sodium anion of **30** with either a preformed phenylcarbamate or a commercially available isocyanate. The aminopyrazoles and aminoisoxazoles **31** that were not commercially available were prepared as described previously.[23,24] The Boc protecting group was then removed upon treatment with TFA to provide the desired compounds **33** for testing against VEGFR-2.

Compound Evaluation. *In vitro* inhibition of VEGFR-2 receptor tyrosine kinase was assessed with two primary assays: a KDR receptor tyrosine kinase biochemical assay and a cellular assay with BaF3-Tel-KDR cells that are engineered to constitutively require VEGFR-2 kinase domain activity for survival and proliferation. Select compounds were evaluated for selectivity in a panel of 62 kinases.

Early in our effort, it was found that some of the compounds also inhibited hERG, which is a potassium ion channel that can cause long QT syndrome and cardiac dysfunction. As we aimed to minimize the associated systemic risk, compounds were analyzed in an automated Q-patch assay to determine their activity on the hERG channel.[25]

Scheme 6[a]

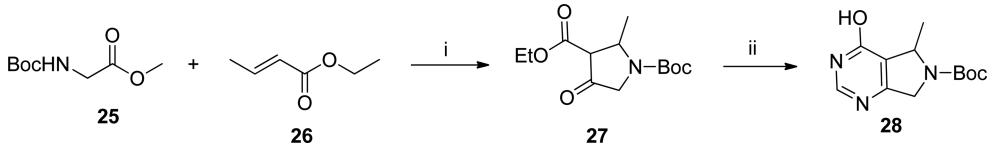

[a]Reagents and conditions: (i) NaH, toluene, 0 °C to rt; (ii) formamidine acetate, EtONa, EtOH, reflux, ∼ 20%.

DOI: 10.1021/acs.jmedchem.5b01227
J. Med. Chem. 2015, 58, 9273−9286

As we sought to identify compounds that selectively distributed to the ocular tissues, we did not apply the usual *in vitro* PK-ADME filters prior to *in vivo* evaluation. Priority was given to compounds that had demonstrated good aqueous solubility,[26] yet generally those with good *in vitro* potency were selected for evaluation in the mouse laser CNV model (C57BL/6) at a single dose of 10 mg/kg (p.o.). This screening dose was selected based on early efficacy studies with existing VEGFR-2 inhibitors, such as **1**, and was not expected to cause any acute side effects that would compromise a given study. Compounds were formulated as suspensions (0.5% methyl cellulose, Tween 80, and water) to better inform our understanding of their intrinsic ADME properties. Each compound was dosed starting the day of laser application and continued daily with the last dose given on day 6 and CNV area measurement on day 7. Comparison of CNV area in animals dosed with compound or placebo was used to establish percent inhibition.

Compounds exhibiting >60% inhibition at the 10 mg/kg screening dose were further evaluated in mouse CNV dose–response studies to establish ED_{50} and ED_{90} relationships. Compounds with an ED_{90} < 20 mg/kg in the mouse CNV assay were then characterized in the rat laser CNV model (Brown Norway). To understand the correlation between efficacy and exposure, the distribution profiles for select compounds were determined by orally dosing Brown Norway rats and measuring time course drug exposures in the plasma and ocular tissues (retina and retinal pigment epithelium/choroid/sclera complex). Further understanding of the ADME profiles for select compounds was accomplished by discrete i.v./p.o. PK studies in Brown Norway rats.

RESULTS

Early on, we recognized the need to improve on the aqueous solubility of compound **1**. It was anticipated that greater aqueous solubility would provide increased oral bioavailability and as a consequence better efficacy. X-ray cocrystal structures of related VEGFR-2 inhibitors indicated that incorporation of ionizable groups on the pyrimidine should be possible. An important early finding was that the aminopyrimidine of **1** was not required for potency as **5a** proved to be equipotent in the biochemical assay and have similar efficacy in the mouse CNV model (Table 1; 45% inhibition). A basic amine was introduced to give compound **6a**, which demonstrated similar potency *in vitro* and importantly increased efficacy *in vivo* (67% inhibition). As anticipated, **6a** had improved aqueous solubility (Table 2; 64 μM) relative to that of **1**. Incorporation of a fluoro substituent in the 4-position of the aniline as in **6b** provided a boost in efficacy as the compound showed 92% inhibition of neovascularization in the mouse at the 10 mg/kg dose.

Collectively, these compounds demonstrated the potential for optimization through inclusion of the basic amine moiety; however, **6b** was found to have an undesirable level of activity on the hERG channel (Table 3; IC_{50} 5800 nM). To optimize *in vivo* efficacy while balancing hERG activity and aqueous solubility, we focused our efforts on the basic amine region and the urea side chain of **6b**. Our exploration centered on altering both the pK_a and the steric environment of the amine as well as reducing the lipophilicity of the urea side chain. It was thought that a combination of these changes would provide the desired efficacy while reducing hERG liability.

Rigidification of the amine side chain by incorporation into the 6,6-bicyclic pyrimidine **33a** was well tolerated as it gave 87% inhibition in the mouse CNV model with modest aqueous solubility (84 μM). However, no substantial reduction in hERG activity was realized (IC_{50} 8900 nM). Intriguingly, the isomeric 6,6-bicyclic pyrimidine **33b** provided no significant inhibition *in vivo* despite having good potency in the enzymatic and cellular assays.

To further probe the sensitivity of this region to substitution, the enantiomeric methyl analogues **33c** and **33d** were prepared. These compounds again highlighted a similar pattern of disconnect between the *in vitro* and the *in vivo* efficacy as **33c**, the (*S*)-enantiomer, demonstrated greater efficacy despite similar *in vitro* potency to the (*R*)-enantiomer **33d**. Acetylation of the amine as in **33e** caused a complete loss of efficacy in the mouse model, while retention of the basic amine as in the ethyl derivative **33f** provided 81% inhibition. However, the tertiary amine **33f** reduced the aqueous solubility (<5 μM).

Reduction of amine pK_a was achieved with the 6,5-bicyclic pyrimidine **33g**. This compound was found to be efficacious (68% inhibition) in the mouse model and demonstrated reduced hERG activity (IC_{50} 15600 nM). In this instance, however, the addition of a methyl group to the bicycle as in **33h** and **33i** attenuated the efficacy.

The pyridyl analogue **33j** was designed to reduce the lipophilicity of the aniline moiety. Although the *in vitro* potency in both the biochemical (280 nM) and cell (1922 nM) assays

Table 2. Comparison of Aqueous Solubility for Selected VEGFR-2 Inhibitors

cmpd	aq sol pH 6.8 (μM)[a]
1	< 5
6a	64
33a	84
33f	<5
33j	190
33k	833
33l	682
33m	252
33n	450
33o	489
33q	167
33r	126
33s	20
33t	232
33v	110
33w	37

[a]Aqueous high-throughput equilibrium solubility (see ref 26).

Table 3. Comparison of hERG Activity for Selected VEGFR-2 Inhibitors

cmpd	hERG IC_{50} (nM)[a]
6b	5800
33a	8900
33c	10700
33g	15600
33m	>30000
33n	27400
33q	7000
33r	11100
33s	23500
33v	>30000

[a]Automated Q-patch assay.

DOI: 10.1021/acs.jmedchem.5b01227
J. Med. Chem. 2015, 58, 9273–9286

was attenuated, it demonstrated the potential benefit through further optimization to identify more preferred heteroaryl groups as there was a favorable impact on aqueous solubility (190 μM). Indeed, further design of heteroaryl replacements led to pyrazoles **33k** and **33l** that provided very good *in vitro* potency (cell IC_{50} 3 nM and 1 nM, respectively). While the initial pyrazole analogues **33k** and **33l** provided no inhibition in the mouse CNV model, they did have markedly improved aqueous solubility (833 and 682 μM, respectively). Further design and optimization led to the discovery that the cyclopropylmethyl analogue **33m** provided 64% inhibition. The close structural similarities among these analogues again provide a dramatic demonstration of the subtle effects realized only with *in vivo* SAR. Pyrazole **33m** had good aqueous solubility (252 μM) and minimal hERG activity with an IC_{50} > 30,000 nM. This was an important finding as it demonstrated the ability to reduce hERG activity without alteration of the amine basicity.

Combining the methyl substituted 6,6-bicyclic pyrimidine with the cyclopropylmethyl pyrazole as in **33n** gave good potency in the cellular assay (0.9 nM), efficacy in the mouse (67% inhibition), good aqueous solubility (450 μM), and minimal hERG activity (IC_{50} 27,400 nM). In this case, as shown above, the opposite enantiomer **33p** and the 6,5-bicyclic analogue **33o** showed reduced efficacy *in vivo* despite similar potency *in vitro*.

Further exploration of aniline replacements revealed that the isoxazole (e.g., **33q** and **33r** with 83% and 96% inhibition, respectively) provided even greater efficacy than the corresponding pyrazole analogues; however, they also had greater hERG activity. It was also found that the 3-aminoisoxazole analogues (e.g., **33s**) were more active *in vivo* than the isomeric 5-aminoisoxazoles (e.g., **33t**). Similar to the pyrazole analogues, inclusion of the methyl group in 6,5-pyrimidine did not give a favorable increase in activity (**33u**), which was again in contrast to the 6,6-bicyclic pyrimidines. Modification of the isoxazole substitution from *t*-butyl to cyclopropyl **33v** or isopropyl **33w** provided maximal inhibition in the mouse model (98 and 96% inhibition, respectively). Isoxazole **33v** also showed minimal hERG activity with an IC_{50} > 30,000 nM in combination with good aqueous solubility (110 μM).

Dose–response studies in the mouse and rat were conducted for the preferred compounds identified from the mouse *in vivo* single dose screen (Table 4). In the mouse laser CNV model, the isoxazole derivative **33v** provided the greatest efficacy on a per dose basis with an ED_{90} of 4.8 mg/kg, while its corresponding aniline analogue **33g** provided an ED_{90} of 31 mg/kg. In contrast, the pyrazole analogue **33n** was found to have a higher ED_{90} (19.6 mg/kg) than its corresponding aniline derivative **33c** in the mouse CNV. Both the nonmethylated **33m** and the methylated **33n** provided a similar dose–response in the mouse model. Further characterization of **33n**, **33v**, and **33m** in the rat laser CNV model again demonstrated that on a per dose basis **33v** was more efficacious than either **33m** or **33n**.

Table 4. Dose–Response Inhibition of Laser Induced Choroidal Neovascularization for Selected VEGFR-2 Inhibitors

	mouse[a]		rat[b]	
cmpd	ED_{50} (mg/kg)	ED_{90} (mg/kg)	ED_{50} (mg/kg)	ED_{90} (mg/kg)
33c	3.6	8.5		
33g	6.9	31		
33n	3.4	19.6	2.9	14.6
33v	1.8	4.8	0.7	2.7
33m	7.8	25.3	2.7	13.6

[a]Compounds dosed q.d. orally as 0.5% MC/0.1% Tween 80, WFI 7 days. [b]Compounds dosed q.d. orally as 0.5% CMC/0.1% Tween 80, WFI 14 days.

As stated above, our key objective was to identify VEGFR-2 inhibitors that provided good efficacy in the mouse and rat laser CNV models following oral dosing and demonstrated distribution to and retention in the ocular tissues relative to the plasma. Discrete oral PK studies in Brown Norway rats were conducted with preferred compounds. Exposure in plasma, retina, and posterior eye cup (retinal pigment epithelium/choroid sclera complex = posterior eye cup) were assessed at 7 time points after dosing between 0 and 24 h. In Table 5, the dose normalized (DN) exposures for 3 compounds are detailed. It can readily be seen that **33v** has significantly higher plasma exposure (DNC_{max} and DNAUC) than either **33n** or **33m**. In the retina, **33n** and **33v** had similar exposure, while **33m** was measurably lower. In the PEC, there was even greater contrast among the three compounds with the exposure decreasing in order from **33v** > **33n** > **33m**. The data from the ocular tissues indicate a strong preference for the retention of each of the compounds in those tissues versus retention in the plasma. This is most easily noted by comparison of the plasma/retina/PEC dose normalized concentrations at 24 h (**33n**, 1.6/122/1067 nM; **33v**, 6/65/3334 nM; **33m**, 0.7/13/102 nM). The above data demonstrate that it is possible to identify compounds with preferential distribution to the ocular tissues and reduced plasma exposure. The advantage of such distribution in mitigating systemic side effects will only be borne out in toxicology studies as it was not expected that our efficacy models would address this. However, it is worth noting that the approved VEGFR-2 inhibitor pazopanib, described above, has been reported to provide 93% inhibition of laser-induced CNV in the mouse model when dosed orally at 100 mg/kg twice daily and that dose when given for 7 d produced a plasma exposure of ~13 μM at 16 h post the last dose.[27]

The i.v./p.o. PK parameters of **33n**, **33v**, and **33m** provide further details regarding systemic exposure and clearance (Table 6). In accord with the ocular PK study above, **33m** shows a higher rate of clearance from the plasma (165 mL/min/kg), while **33v** provided much lower clearance (6 mL/min/kg). All three of these compounds were found to have good plasma exposure following oral dosing (F% > 50). The plasma and ocular PK data highlight the limitation of optimizing compounds with limited *in vivo* efficacy measurements or an over reliance on *in vivo* PK as **33m** would not have been preferred either from plasma or ocular PK, yet the compound is efficacious at reducing laser-induced CNV.

In a selectivity panel consisting of 62 kinases, **33n** and **33v** were found to have activity <1 μM against several related kinases [IC_{50} (μM) **33n**, Ret 0.066, PDGFRα 0.15, and c-Kit 0.6; **33v**, Ret 0.50, PDGFRα 0.15 μM]. This is consistent with the observed *in vivo* efficacy being primarily driven by VEGFR-2 inhibition.

CONCLUSIONS

Predicting ocular efficacy based on *in vitro* potency and *in vivo* exposure remains a challenge in ocular drug discovery. This is in part evidenced by the high number of potent VEGFR-2

DOI: 10.1021/acs.jmedchem.5b01227
J. Med. Chem. 2015, 58, 9273–9286

Table 5. Dose Normalized (DN) Exposure in Selected Tissues from Brown Norway Rats for Selected VEGFR-2 Inhibitors 33n, 33m, and 33v[a]

tissue	cmpd	$DNAUC_{PO\ 0-24h}$ (nM·h/mg/kg)	DNC_{Max} (nM/mg/kg)	DNC_{24h} (nM/mg/kg)
plasma	**33n**	598	68	1.6
	33v	15014	3225	6
	33m	166	33	0.7
retina	**33n**	3215	170	122
	33v	2692	337	65
	33m	310	15	13
PEC	**33n**	22266	1067	1067
	33v	92954	5293	3344
	33m	2386	110	102

[a]Each compound was dosed orally as a suspension of 0.5% MC/0.1% Tween 80, WFI at the following doses: 6 mg/kg (ED_{50} = 3.0 mg/kg) (33n); 6 mg/kg (ED_{50} = 2.7 mg/kg) (33m); and 2 mg/kg (ED_{50}= 0.7 mg/kg) (33v). PEC = posterior eye cup (retinal pigment epithelium/choroid/sclera complex).

Table 6. PK-ADME Parameters for Selected VEGFR-2 Inhibitors.[a]

parameter	33n[b,d,f]	33v[b,e,f]	33m[c,d,f]
$AUC_{PO\ 0-8h}$ (μM·h)	2488	29393	1121
CL (mL/min/kg)	27	6	165
Vdss (L/kg)	5.6	0.5	22
$t_{1/2}$ (h)	2.3	1.2	2.7
C_{max} (nM)	514	11003	505
F (%)	81	100	51

[a]Brown Norway rat PK. Animals were dosed i.v. at 1 mg/kg, n = 2. [b]Animals were dosed p.o. at 3 mg/kg, n = 3. [c]Animals were dosed p.o. at 10 mg/kg, n = 3. [d]i.v. dose: 10% NMP, 15% PG, 4% cremophorEL, and PBS. [e]i.v. dose: 10% NMP, 30% PEG 300, and 60% WFI. [f]p.o. dose: 0.5% MC/0.1% Tween 80. WFI PK parameters are derived from p.o. dosing and are reported as the mean ± SD.

inhibitors described herein, which provide little or no efficacy in the mouse laser CNV model. The challenge is more clearly illustrated by molecules **33m**, **33n**, and **33v**, which provide similar *in vivo* efficacy despite substantially different tissue distribution profiles. The reasons for these disconnects are not fully understood at this time. We believe melanin binding plays a key role not only in the preferential distribution of the compound to the ocular tissue but also in the differing correlations between ocular exposure and efficacy in the CNV models. In part, the answer may come from melanin binding studies that adequately provide the kinetic binding profiles of the molecules. Differential kinase selectivity may provide another hypothesis to explain the exposure−efficacy disconnect, although data collected against a kinase panel indicate that the molecules are reasonably selective for VEGFR-2 and have similar broad profiles.

Despite the inability to *a priori* predict ocular efficacy based on plasma PK and potency, our use of relatively high-throughput *in vivo* screening in a mouse laser CNV model facilitated the generation of clear and actionable *in vivo* SAR. Through optimization of one particular series of VEGFR-2 inhibitors, described herein, multiple promising compounds were identified that effectively reduced choroidal neovascularization and provided preferential distribution to the ocular tissues. The observations made with **33m**, **33n**, and **33v** are a clear demonstration of the ability to identify VEGFR-2 inhibitors with markedly higher ocular exposure than that in the plasma. Selective distribution to the target tissue of interest, the eye in this case, may provide an advantage in minimizing systemic side effects. This is of particular interest as the on-target systemic toxicity of VEGFR-2 inhibitors has been well established and thus may be a barrier to systemic use of such therapy in the treatment of AMD. This data may support the potential clinical utility of systemically administered VEGFR-2 inhibitors with preferential ocular distribution as a therapy for wet AMD. A similar strategy may be applicable to other disease indications that would benefit from local drug distribution to limit systemic toxicity.

EXPERIMENTAL SECTION

Chemistry: General. NMR spectra were recorded on a Bruker Avance II 400 MHz spectrometer. All chemical shifts are reported in parts per million (δ) relative to tetramethylsilane. The following abbreviations are used to denote signal patterns: s = singlet, d = doublet, t = triplet, m = multiplet, and br = broad. Flash chromatography was conducted using grade 60 230−400 mesh silica gel from Fisher Chemical (S825-1) or by utilizing the CombiFlash Companion from Teledyne Isco, Inc. and RediSep Rf disposable normal phase silica gel columns (4−300 g). Thin layer chromatography was performed using 2.5 × 7.5 cm glass-backed TLC Silica Gel 60 F_{254} plates from EMD Chemicals, Inc. (15341-1) and visualized by UV light. HPLC purifications were performed on a Gilson preparative HPLC system controlled by Unipoint software using X-Bridge Phenyl, C8, C18, or RP18 30 × 50 mm columns with 5 μm particle size. The purity of all compounds was ≥95%, unless otherwise noted. Low-resolution mass spectra were recorded using an Agilent 1100 series LC-MS spectrometer.

*5-(6-Benzyloxymethyl-pyrimidin-4-yloxy)-1H-indole (**4**).* 5-Hydroxy indole **2** (5 g, 37.6 mmol) was added in one portion to a solution of 4-(benzyloxymethyl)-6-chloropyrimidine **3** (8.81 g, 37.6 mmol) and DBU (5.66 mL, 37.6 mmol) in ACN (107 mL) at room temperature. This was stirred overnight for 20 h. The reaction was concentrated and purified via FCC (12−100% EtOAc/heptane) to obtain the title compound (9.37 g, 28.3 mmol, 75% yield). MS (ESI) m/z 447.0 (M + 1); ^{1}H NMR (400 MHz, DMSO-d_6) δ 11.11−11.44 (m, 1 H), 8.58−8.82 (m, 1 H), 7.41−7.51 (m, 2 H), 7.34−7.39 (m, 1 H), 7.21−7.32 (m, 5 H), 6.88−6.94 (m, 2 H), 6.42−6.50 (m, 1 H), 4.52−4.64 (m, 4 H).

*5-(6-Hydroxymethyl-pyrimidin-4-yloxy)-indole-1-carboxylic Acid (4-Fluoro-3-trifluoromethyl-phenyl)-amide (**5**).* To NaH (255 mg, 6.37 mmol) in 40 mL of DMF at 0 °C under nitrogen was added a solution of 5-(6-(benzyloxymethyl)pyrimidin-4-yloxy)-1*H*-indole (960 mg, 2.90 mmol) in 5 mL of DMF and stirred at 0 °C for 0.5 h. The reaction was then cooled to −50 °C, followed by the addition of 1-fluoro-4-isocyanato-2-(trifluoromethyl)benzene (0.454 mL, 3.19 mmol) in 5 mL of DMF. The cold bath was removed,and the reaction allowed to warm to RT. After 3 h, the reaction was quenched with NH_4Cl, extracted 2× EtOAc, and the combined organics washed with H_2O (3×), brine, dried over Na_2SO_4, and concentrated. The residue was then purified via FCC (1−50% EtOAc/CH_2Cl_2) to obtain

DOI: 10.1021/acs.jmedchem.5b01227
J. Med. Chem. 2015, 58, 9273−9286

5-((6-((benzyloxy)methyl)pyrimidin-4-yl)oxy)-*N*-(4-fluoro-3-(trifluoromethyl)phenyl)-1*H*-indole-1-carboxamide (1.36 g, 2.54 mmol, 88% yield). MS (ESI) *m*/*z* 537.0 (M + 1); ^{1}H NMR (400 MHz, DMSO-d_6) δ 10.40 (s, 1 H), 8.69 (s, 1 H), 8.30 (d, *J* = 8.84 Hz, 1 H), 8.07−8.19 (m, 2 H), 7.96−8.06 (m, 1 H), 7.58 (t, *J* = 9.85 Hz, 1 H), 7.52 (d, *J* = 2.27 Hz, 1 H), 7.24−7.40 (m, 5 H), 7.17 (dd, *J* = 8.97, 2.40 Hz, 1 H), 7.02 (s, 1 H), 6.82 (d, *J* = 3.79 Hz, 1 H), 4.61 (d, *J* = 8.84 Hz, 4 H).

A solution of 5-((6-((benzyloxy)methyl)pyrimidin-4-yl)oxy)-*N*-(4-fluoro-3-(trifluoromethyl)phenyl)-1*H*-indole-1-carboxamide (1.48 g, 2.76 mmol) in TFA (15 mL) was heated at 100 °C for 4 h before concentrating and absorbing onto silica to purify via FCC 10−100% EtOAc/CH_2Cl_2 10CV, then 100% EtOAc to provide the title compound **5** (0.915 g, 2.052 mmol, 74% yield). MS (ESI) *m*/*z* 447.0 (M + 1); ^{1}H NMR (400 MHz, DMSO-d_6) δ 10.40 (s, 1 H), 8.65 (d, *J* = 1.01 Hz, 1 H), 8.29 (d, *J* = 9.09 Hz, 1 H), 8.09−8.12 (m, 2H), 8.99−8.04 (m, 1 H), 7.58 (t, *J* = 9.60 Hz, 1 H), 7.51 (d, *J* = 2.53 Hz, 1 H), 7.16 (dd, *J* = 8.84, 2.53 Hz, 1 H), 6.99 (d, *J* = 1.01 Hz, 1 H), 6.82 (d, *J* = 3.79 Hz, 1 H), 5.61 (t, *J* = 5.05 Hz, 1 H), 4.52 (d, *J* = 5.05 Hz, 2 H).

*5-(6-Methylaminomethyl-pyrimidin-4-yloxy)-indole-1-carboxylic Acid (4-Fluoro-3-trifluoromethyl-phenyl)-amide (**6b**).* To a solution of 5-(6-hydroxymethyl-pyrimidin-4-yloxy)-indole-1-carboxylic acid (4-fluoro-3-trifluoromethyl-phenyl)-amide **5** (260 mg, 0.6 mmol), methanesulfonic anhydride (240 mg, 1.4 mmol), and THF (15 mL) was added pyridine (0.2 mL). The mixture was stirred at rt for 0.5 h before being filtered. The filtrate was used in the next step without purification. MS (ESI) *m*/*z* 525.0 (M + 1).

To a solution of 5-(6-methanesulfonylmethyl-pyrimidin-4-yloxy)-indole-1-carboxylic acid (4-fluoro-3-trifluoromethyl-phenyl)-amide ((270 mg, 0.515 mmol) was added methyl amine (8 mL, 2.0 M in methanol). The mixture was stirred at room temperature for 16 h, then concentrated under reduced pressure. The residue was diluted with EtOAc and washed with water and brine. The organic layer was removed, dried, and concentrated. The residue was then separated by FCC (MeOH with 1% NH_4OH/DCM from 0% to 10%) to give the title compound **6b** (127 mg, 0.276 mmol, 54%). MS (ESI) *m*/*z* 460.1 (M + 1); ^{1}H NMR (400 MHz, methanol-d_4) δ 8.65 (d, *J* = 1.01 Hz, 1 H), 8.35 (d, *J* = 8.84 Hz, 1 H), 8.04 (dd, *J* = 6.19, 2.65 Hz, 1 H), 7.90−7.94 (m, 2 H), 7.41 (d, *J* = 2.27 Hz, 1 H), 7.35 (t, *J* = 9.60 Hz, 1 H), 7.11 (dd, *J* = 8.97, 2.40 Hz, 1 H), 7.00 (s, 1 H), 6.74 (d, *J* = 3.79 Hz, 1 H), 3.82 (s, 2 H), 2.43 (s, 3 H).

*5-(6-Methylaminomethyl-pyrimidin-4-yloxy)-indole-1-carboxylic Acid (3-Trifluoromethyl-phenyl)-amide (**6a**).* Prepared as described for **6b**. MS (ESI) *m*/*z* 442.1 (M + 1); ^{1}H NMR (400 MHz, methanol-d_4) δ 8.64 (s, 1 H), 8.34 (d, *J* = 9.09 Hz, 1 H), 8.05 (s, 1 H), 7.93 (d, *J* = 3.79 Hz, 1 H), 7.89 (d, *J* = 8.08 Hz, 1 H), 7.56 (t, *J* = 7.96 Hz, 1 H), 7.40−7.46 (m, 2 H), 7.10 (dd, *J* = 8.97, 2.40 Hz, 1 H), 6.99 (s, 1 H), 6.73 (d, *J* = 3.79 Hz, 1 H), 3.77 (s, 2 H), 2.40 (s, 3 H).

*4-Chloro-5,8-dihydro-6H-pyrido[3,4-d]pyrimidine-7-carboxylic Acid tert-Butyl Ester (**8**).* 7-Benzyl-5,6,7,8-tetrahydro-3*H*-pyrido[3,4-*d*]pyrimidin-4-one[28] (36.9 g, 153 mmol) and BOC anhydride (40.1 g, 184 mmol) were taken up in MeOH (600 mL). The vessel was purged with argon, and palladium on carbon (10% w/w; wet) (5.0 g) was added. The contents were then stirred under a hydrogen atmosphere (1 atm) for 18 h. At that time, the suspension was filtered over Celite, and the resulting solution was concentrated to give the title compound, which was taken to the next step without further purification. MS (ESI) *m*/*z* 252.0 (M + 1); ^{1}H NMR (400 MHz, DMSO-d_6) δ 12.41 (s, 1H), 8.04 (s, 1H), 4.22 (s, 2H), 3.51 (app t, *J* = 5.7 Hz, 2H), 2.40 (app t, *J* = 5.7 Hz, 2H), 1.42 (s, 9H).

Triphenylphosphine (17.3 g, 66.1 mmol) was added to a solution of 4-oxo-4,5,6,8-tetrahydro-3*H*-pyrido[3,4-*d*]pyrimidine-7-carboxylic acid *tert*-butyl ester (8.30 g, 33.0 mmol), CCl_4 (9.6 mL, 99 mmol), and 1,2-dichloroethane (250 mL). The solution was heated at 70 °C for 2.5 h. The solution was concentrated *in vacuo* to about 50 mL. The contents of the flask were then filtered over a silica gel plug eluting with 60% EtOAc/heptane. The residue following concentration was then further separated via flash chromatography (10−30% EtOAc/heptane) to give the title compound **8** (7.09 g, 26.3 mmol, 80%). MS (ESI) *m*/*z* 270.0 and 272.0 (M + 1); ^{1}H NMR (400 MHz, chloroform-*d*) δ 8.79 (s, 1 H), 4.65 (s, 2 H), 3.74 (t, *J* = 5.8 Hz, 2 H), 2.87 (t, *J* = 5.8 Hz, 2 H), 1.49 (s, 9 H).

*tert-Butyl 4-chloro-7,8-dihydropyrido[4,3-d]pyrimidine-6(5H)-carboxylate (**10**).* Prepared as described for **8**. MS (ESI) *m*/*z* 270.0 and 271.9 (M + 1); ^{1}H NMR (400 MHz, chloroform-*d*) δ 8.79 (s, 1H), 4.58 (s, 2H), 3.76 (t, *J* = 5.9 Hz, 2H), 2.97 (t, *J* = 5.8 Hz, 2H), 1.50 (s, 9H).

*4-[Benzyl-(1-ethoxycarbonyl-ethyl)-amino]-butyric Acid Methyl Ester (**13**).* Ethyl alanine hydrochloride (5.5 g, 36.8 mmol), benzaldehyde (7.9 mL, 77.8 mmol), TEA (10.8 mL, 77.8 mmol), and $NaBH(OAc)_3$ (16.5 g, 77.8 mmol) were taken up in 1,2-DCE (200 mL) and stirred at rt for 4 h. The reaction was then partitioned between DCM and saturated aqueous $NaHCO_3$. The organic layer was removed, dried over anhydrous Na_2SO_4, and concentrated *in vacuo*. The crude residue was used without further purification. MS (ESI) *m*/*z* 208.2 (M + 1).

2-Benzylamino-propionic acid ethyl ester (1.4 g, 6.7 mmol), methyl oxo-butanoate (1.7 g, 13.5 mmol), TEA (1.9 mL, 13.5 mmol), and $NaBH(OAc)_3$ (2.9 g, 13.5 mmol) were taken up in 1,2-DCE (35 mL) and stirred at rt for 4 h. The reaction was partitioned between DCM and saturated aqueous $NaHCO_3$. The organic layer was removed, dried over anhydrous Na_2SO_4, and concentrated *in vacuo*. The crude residue was used without further purification. MS (ESI) *m*/*z* 308.3 (M + 1).

*1-Benzyl-2-methyl-3-oxo-piperidine-4-carboxylic Acid Methyl Ester (**14**).* A mixture of 4-[benzyl-(1-ethoxycarbonyl-ethyl)-amino]-butyric acid methyl ester (1.5 g, 4.9 mmol), potassium *tert*-butoxide (906 mg, 8.9 mmol), and toluene (100 mL) was stirred at rt for 3 h. The mixture was then partitioned between DCM and saturated aqueous NH_4Cl. The organic layer was removed, dried over anhydrous Na_2SO_4, and concentrated. The crude residue was used without further purification. MS (ESI) *m*/*z* 262.2 (M + 1).

*4-Chloro-8-methyl-5,8-dihydro-6H-pyrido[3,4-d]pyrimidine-7-carboxylic Acid tert-Butyl Ester (**15**).* Prepared as described for **8**. MS (ESI) *m*/*z* 284.2 (M + H); ^{1}H NMR (400 MHz, methylene chloride-d_2) δ 8.67 (s, 1H), 5.24−5.23 (m, 2H), 5.05 (s, 1H), 4.26 (s, 1H), 2.97 (s, 1H), 1.42 (d, *J* = 6.9 Hz, 3H), 1.39 (s, 9H).

*Ethyl 4-((2-Ethoxy-2-oxoethyl)((S)-1-phenylethyl)amino)-pentanoate (**18**).* To a solution of (*S*)-1-phenylethanamine (25.0 g, 206 mmol) and $NaBH(OAc)_3$ (65.6 g, 309 mmol) in 1,2-DCE (500 mL) was added ethyl levulinate (29.4 mL, 206 mmol). The reaction was stirred at room temperature for 16 h. The mixture was then partitioned between DCM and saturated aqueous $NaHCO_3$. The organic layer was removed, and the aqueous layer was extracted further with DCM (2×). The combined organic layers were then dried over anhydrous Na_2SO_4, filtered, and concentrated under reduced pressure. The crude ethyl 4-((*S*)-1-phenyl-ethyl)amino)pentanoate was used without further purification. MS (ESI) *m*/*z* 250.2 (M + 1).

To a solution of ethyl 4-((*S*)-1-phenylethylamino)pentanoate (51.4 g, 206 mmol) and $NaBH(OAc)_3$ (65.5 g, 309 mmol) in 1,2-DCE (500 mL) was added ethyl glyoxylate (84 g, 412 mmol, 50% toluene solution). The reaction was stirred at room temperature for 18 h. The mixture was then partitioned between DCM and saturated aqueous $NaHCO_3$. The organic layer was removed, and the aqueous layer was extracted further with DCM (2×). The combined organic layers were then dried over anhydrous Na_2SO_4, filtered, and concentrated under reduced pressure. The crude diastereomeric mixture of ethyl 4-((2-ethoxy-2-oxoethyl)((*S*)-1-phenylethyl)amino)pentanoate (**18**) was used without further purification. MS (ESI) *m*/*z* 336.4 (M + 1).

*(2S)-Ethyl 2-Methyl-5-oxo-1-((S)-1-phenylethyl)piperidine-4-carboxylate (**19**) and (2R)-Ethyl 2-methyl-5-oxo-1-((S)-1-phenylethyl)-piperidine-4-carboxylate (**20**).* To a solution of ethyl 4-((2-ethoxy-2-oxoethyl)((*S*)-1-phenylethyl)amino)pentanoate (44.5 g, 133 mmol) in toluene (500 mL) was added KO*t*Bu (37.2 g, 332 mmol). After stirring for 3 h at room temperature, the mixture was then partitioned between DCM and saturated aqueous NH_4Cl. The organic layer was removed, and the aqueous layer was extracted further with DCM (2×). The combined organic layers were then dried over anhydrous Na_2SO_4, filtered, and then concentrated under reduced pressure. The crude

DOI: 10.1021/acs.jmedchem.5b01227
J. Med. Chem. 2015, 58, 9273−9286

residue was purified via FCC (2.5% EtOAc/heptane) to give both of the title diastereomers (**19**, 20.6 g, 54%; **20**, 7.5 g, 19%). Analytical data for **19**: MS (ESI) *m/z* 290.2 (M + 1); ^{1}H NMR (400 MHz, chloroform-*d*) δ 11.81 (s, 1 H), 7.18−7.37 (m, 5 H), 4.16−4.27 (m, 2 H), 3.70 (q, *J* = 6.6 Hz, 1 H), 3.27−3.38 (m, 1 H), 2.82−3.13 (m, 2 H), 2.53 (dd, *J* = 15.5, 5.2 Hz, 1 H), 2.10 (dd, *J* = 15.5, 3.7 Hz, 1 H), 1.33 (d, *J* = 6.6 Hz, 3 H), 1.30 (t, *J* = 7.1 Hz, 3 H), 1.05 (d, *J* = 6.6 Hz, 3 H). Analytical data for **20**: MS (ESI) *m/z* 290.2 (M + 1); ^{1}H NMR (400 MHz, $CDCl_3$) δ 11.94 (s, 1 H), 7.19−7.36 (m, 5 H), 4.13−4.29 (m, 2 H), 3.63 (q, *J* = 6.6 Hz, 1 H), 3.09−3.52 (m, 2 H), 2.94−3.05 (m, 1 H), 2.34−2.47 (m, 1 H), 1.94 (d, *J* = 15.4 Hz, 1 H), 1.34 (d, *J* = 6.6 Hz, 3 H), 1.28 (t, *J* = 7.2 Hz, 3 H), 0.90 (d, *J* = 6.8 Hz, 3 H).

*(S)-tert-Butyl 4-Chloro-6-methyl-5,6-dihydropyrido[3,4-d]-pyrimidine-7(8H)-carboxylate (**21**).* A combination of (2*S*)-ethyl 2-methyl-5-oxo-1-((*S*)-1-phenylethyl)piperidine-4-carboxylate **19** (20.6 g, 71.2 mmol), formamidine acetate (11.1 g, 107 mmol), and EtOH (250 mL) was treated with NaOEt solution (57.7 g, 178 mmol, 21% w/w EtOH solution) and then heated at 90 °C for 4 h. At that point, the solvent was removed under reduced pressure, and the residue was taken up in DCM and washed with sat aq NH_4Cl. The aqueous layer was further extracted with DCM, and the combined organic layers were then dried over sodium sulfate, filtered, and concentrated to give (*S*)-6-methyl-7-((*S*)-1-phenylethyl)-5,6,7,8-tetrahydropyrido[3,4-*d*]-pyrimidin-4(3*H*)-one, which was taken to the next step without further purification. MS (ESI) *m/z* 270.1 (M + 1).

To a mixture of (*S*)-6-methyl-7-((*S*)-1-phenylethyl)-5,6,7,8-tetrahydropyrido[3,4-*d*]pyrimidin-4(3*H*)-one (20.0 g, 74.3 mmol), ammonium formate (23.4 g, 371 mmol) and BOC-anhydride (48.6 g, 223 mmol), in EtOH (300 mL), was added 20% $Pd(OH)_2$/C (7.82 g, 50% wet), and the reaction was heated at reflux for 1 h. The mixture was then filtered through a Celite pad, and the filterate was concentrated. The residue was purified via FCC (0−5% MeOH/DCM) to give (*S*)-*tert*-butyl 6-methyl-4-oxo-3,4,5,6-tetrahydropyrido-[3,4-*d*]pyrimidine-7(8*H*)-carboxylate (15.7 g, 80%). MS (ESI) *m/z* 266.1 (M + H); ^{1}H NMR (400 MHz, chloroform-*d*) δ 12.70 (s, 1H), 8.09 (s, 1H), 4.85−4.65 (m, 2H), 4.03 (d, *J* = 19.8 Hz, 1H), 2.70 (dd, *J* = 17.2, 6.0 Hz, 1H), 2.59 (d, *J* = 17.2 Hz, 1H), 1.49 (s, 9H), 1.10 (d, *J* = 6.9 Hz, 3H).

A solution of (*S*)-*tert*-butyl 6-methyl-4-oxo-3,4,5,6-tetrahydropyrido[3,4-*d*]pyrimidine-7(8*H*)-carboxylate, (15.1 g, 57.1 mmol), triphenylphosphine (29.9 g, 114 mmol), and carbon tetrachloride (16.5 mL, 171 mmol) in 1,2-DCE (300 mL) was heated at 70 °C for 3 h. At that time, the solution was concentrated *in vacuo*, and the residue was separated via FCC (5−60% EtOAc/heptane) to give (*S*)-*tert*-Butyl 4-chloro-6-methyl-5,6-dihydropyrido[3,4-*d*]-pyrimidine-7(8*H*)-carboxylate (**21**) (8.22 g, 51%). MS (ESI) *m/z* 284.1 (M + H). ^{1}H NMR (400 MHz, chloroform-*d*) δ 8.78 (s, 1H), 4.96 (d, *J* = 19.7 Hz, 1H), 4.84 (s, 1H), 4.25 (d, *J* = 19.7 Hz, 1H), 2.99 (dd, *J* = 17.1, 5.9 Hz, 1H), 2.74 (d, *J* = 17.1 Hz, 1H), 1.48 (s, 9H), 1.11 (d, *J* = 7.0 Hz, 3H).

*(R)-tert-Butyl 4-Chloro-6-methyl-5,6-dihydropyrido[3,4-d]-pyrimidine-7(8H)-carboxylate (**22**).* Prepared as described for **21**. MS (ESI) *m/z* 284.0 (M + H); ^{1}H NMR (400 MHz, chloroform-*d*) δ 8.81 (s, 1 H) 4.99 (d, *J* = 19.70 Hz, 1 H) 4.86 (br. s., 1 H) 4.27 (d, *J* = 19.96 Hz, 1 H) 3.01 (dd, *J* = 17.18, 6.06 Hz, 1 H) 2.76 (d, *J* = 17.18 Hz, 1 H) 1.41−1.56 (m, 9 H) 1.13 (d, *J* = 6.82 Hz, 3 H).

*4-Oxo-3,4,5,7-tetrahydro-pyrrolo[3,4-d]pyrimidine-6-carboxylic Acid tert-Butyl Ester (**24**).* To a solution of 4-oxo-pyrrolidine-1,3-dicarboxylic acid 1-*tert*-butyl ester 3-ethyl ester (46 g, 179 mmol) in EtOH (1.5 L), formamidine hydrochloride (112 g, 1073 mmol) was added, followed by NaOEt (203 g, 626 mmol). The reaction was heated at 90 °C for 2 h. The reaction mixture was then evaporated, and a saturated solution of ammonium chloride (300 mL) was added followed by DCM (1 L). The layers were separated, and the aqueous layer was extracted further with DCM. The organics were combined, dried, and evaporated to give the crude product. The title compound was purified using silica gel FCC (gradient elution 100% DCM to 94% DCM/6% MeOH) (10 g, 24% yield). ^{1}H NMR (400 MHz, methanol-*d*) δ 8.18 (s, 1 H) 4.47−4.54 (m, 4 H) 1.45−1.56 (m, 8 H) 1.41 (s, 1 H) MS (ESI) *m/z* 238.2 (M + 1).

*5-Methyl-4-oxo-3,4,5,7-tetrahydro-pyrrolo[3,4-d]pyrimidine-6-carboxylic Acid tert-Butyl Ester (**28**).* To a suspension of NaH (9.72 g, 243 mmol, 60% in mineral oil) in toluene (100 mL), ethyl 2-(*tert*-butoxycarbonylamino)acetate (38 g, 187 mmol) was added at 0 °C. The reaction was stirred for 5 h at the same temperature. At that point, ethyl but-2-enoate (25.6 g, 224 mmol) was added, and the reaction allowed to warm up to rt and stirred for a further 2 h. Ethanol (30 mL) was added, and the reaction was then evaporated. The crude 1-*tert*-butyl 3-ethyl 2-methyl-4-oxopyrrolidine-1,3-dicarboxylate was dissolved in EtOH (1500 mL), then formamidine acetate (343 g, 119 mmol) was added followed by sodium ethoxide (47.2 g, 694 mmol). The reaction was left stirring at 90 °C for 8 h. The solvent was then removed, and to the crude material, a saturated solution of NH_4Cl (200 mL) was added followed by DCM (1 L). The water layer was extracted two times with DCM. The organics were dried and evaporated. The crude product was separated by FCC (DCM/MeOH 100:0 to 90:10) to give the title compound (10 g, 21%). MS (ESI) *m/z* 252.2 (M + 1); ^{1}H NMR (400 MHz, MeOD) δ 8.17 (s, 1 H) 4.85−4.92 (m, 1 H) 4.40−4.52 (m, 1 H) 4.02−4.19 (m, 1 H) 1.49−1.51 (m, 12 H).

*4-(1H-Indol-5-yloxy)-5,7-dihydro-pyrrolo[3,4-d]pyrimidine-6-carboxylic Acid tert-Butyl Ester (**30a**).* To a solution of 4-oxo-3,4,5,7-tetrahydro-pyrrolo[3,4-*d*]pyrimidine-6-carboxylic acid *tert*-butyl ester (74 mg, 0.31 mmol) in acetonitrile (3 mL), BOP (179 mg, 0.405 mmol) was added followed by DBU (0.094 mL, 0.624 mmol). After 20 min, 5-hydroxyindole (83 mg, 0.624 mmol) was added. The reaction was left stirring at rt for 3 h. The reaction mixture was evaporated, and the crude product was purified using silica gel FCC (gradient elution: 100% heptane to 60% heptane/40% ethyl acetate) to give the title compound **30a** (70 mg, 64% yield). ^{1}H NMR (400 MHz, DMSO-d_6) δ 11.22 (br. s., 1 H) 8.62 (d, *J* = 4.04 Hz, 1 H) 7.41−7.44 (m, 2 H) 7.35 (d, *J* = 2.27 Hz, 1 H) 6.92 (d, *J* = 8.84 Hz, 1 H) 6.44 (t, *J* = 2.15 Hz, 1 H) 4.56−4.61 (m, 3 H) 4.51 (br. s., 1 H) 1.44−1.51 (m, 9 H) MS (ESI) *m/z* 353.1 (M + 1).

*(S)-4-(1H-Indol-5-yloxy)-6-methyl-5,8-dihydro-6H-pyrido[3,4-d]-pyrimidine-7-carboxylic Acid tert-Butyl Ester (**30b**).* DBU (2.34 mL, 15.5 mmol) was added to a solution of 5-hydroxyindole (2.17 g, 16.3 mmol) and (*S*)-*tert*-Butyl 4-chloro-6-methyl-5,6-dihydropyrido[3,4-*d*]pyrimidine-7(8*H*)-carboxylate (**21**) (2.20 g, 7.75 mmol) in acetonitrile (50 mL) under an argon atmosphere. The reaction was heated at 80 °C for 2.5 h. At that time, the solution was allowed to cool to rt, and the excess solvent was evaporated. The residue was then separated via flash chromatography (30−100% EtOAc) to give the title compound **30b** (2.66 g, 90%). MS (ESI) *m/z* 381.3 (M + 1); ^{1}H NMR (400 MHz, chloroform-*d*) δ 8.53 (s, 1H), 8.22 (s, 1H), 7.43 (d, *J* = 8.7 Hz, 1H), 7.39 (d, *J* = 2.2 Hz, 1H), 6.97 (dd, *J* = 8.7, 2.3 Hz, 1H), 6.56 (t, *J* = 2.3 Hz, 1H), 4.95 (d, *J* = 18.5 Hz, 1H), 4.91−4.82 (m, 1H), 4.24 (d, *J* = 19.1 Hz, 1H), 3.02 (dd, *J* = 16.9, 6.4 Hz, 1H), 2.85 (d, *J* = 16.9 Hz, 1H), 1.51 (s, 9H), 1.20 (d, *J* = 6.9 Hz, 3H).

*3-(1-Methyl-cyclopropyl)-5-phenoxycarbonylamino-pyrazole-1-carboxylic Acid tert-Butyl Ester (**32a**).* To a solution of 5-amino-3-(1-methyl-cyclopropyl)-pyrazole-1-carboxylic acid *tert*-butyl ester[29] (3.90 g, 16.4 mmol) and phenyl chloroformate (3.11 mL, 24.6 mmol) in DCM (150 mL) was added 2,6-lutidine (5.74 mL, 49.3 mmol). After 18 h, the solution was diluted with DCM (100 mL) and washed with 1 M HCl (250 mL). The organic layer was then dried (Na_2SO_4), filtered, and concentrated to provide the title compound (5.07 g, 86% yield). MS (ESI) *m/z* 358.0 (M + 1); ^{1}H NMR (400 MHz, dichloromethane-d_2) δ 9.76 (br. s., 1 H) 7.38−7.45 (m, 2 H) 7.24−7.30 (m, 1 H) 7.16−7.22 (m, 2 H) 6.33 (s, 1 H) 1.57−1.74 (m, 9 H) 1.42 (s, 3 H) 0.89−1.06 (m, 2 H) 0.56−0.84 (m, 2 H).

*5-((S)-6-Methyl-5,6,7,8-tetrahydro-pyrido[3,4-d]pyrimidin-4-yloxy)-indole-1-carboxylic Acid [5-(1-Methyl-cyclopropyl)-2H-pyrazol-3-yl]-amide (**33n**).* Sodium hydride (2.27 g, 56.8 mmol; 60% in oil) was added to a solution of (*S*)-4-(1*H*-indol-5-yloxy)-6-methyl-5,8-dihydro-6*H*-pyrido[3,4-*d*]pyrimidine-7-carboxylic acid *tert*-butyl ester (7.20 g, 18.9 mmol) and 3-(1-methyl-cyclopropyl)-5-phenoxycarbonylamino-pyrazole-1-carboxylic acid *tert*-butyl ester (8.12 g, 22.7 mmol) in THF (250 mL) at 0 °C under argon. After 2 h, the reaction was quenched by slow addition to a stirred solution of saturated

DOI: 10.1021/acs.jmedchem.5b01227
J. Med. Chem. 2015, 58, 9273−9286

aqueous NH_4Cl (1 L), the resulting slurry was then extracted with DCM (3 × 700 mL), and the combined organic layers were dried over sodium sulfate, filtered, and concentrated. The residue was separated directly via FCC (20−50% EtOAc/heptane) to give (*S*)-4-{1-[2-*tert*-butoxycarbonyl-5-(1-methyl-cyclopropyl)-2*H*-pyrazol-3-ylcarbamoyl]-1*H*-indol-5-yloxy}-6-methyl-5,8-*d*ihydro-6*H*-pyrido[3,4-*d*]pyrimidine-7-carboxylic acid *tert*-butyl ester (6.10 g, 50%). MS (ESI) *m*/*z* 644.2 (M + 1); ^{1}H NMR (400 MHz, DMSO-d_6) δ 10.38 (s, 1H), 8.50 (s, 1H), 8.26 (d, *J* = 9.0 Hz, 1H), 7.92 (d, *J* = 3.7 Hz, 1H), 7.49 (d, *J* = 2.4 Hz, 1H), 7.16 (dd, *J* = 8.9, 2.4 Hz, 1H), 6.82 (d, *J* = 3.7 Hz, 1H), 6.37 (s, 1H), 4.79−4.66 (m, 2H), 4.22 (d, *J* = 20.4 Hz, 1H), 2.95 (dd, *J* = 17.1, 6.7 Hz, 1H), 2.79 (d, *J* = 16.8 Hz, 1H), 1.46 (s, 9H), 1.45 (s, 9H), 1.41 (s, 3H), 1.12 (d, *J* = 6.9 Hz, 3H), 0.96 (q, *J* = 4.0 Hz, 2H), 0.82−0.77 (m, 2H).

A solution of (*S*)-4-{1-[2-*tert*-butoxycarbonyl-5-(1-methyl-cyclopropyl)-2*H*-pyrazol-3-ylcarbamoyl]-1*H*-indol-5-yloxy}-6-methyl-5,8-*d*ihydro-6*H*-pyrido[3,4-*d*]pyrimidine-7-carboxylic acid *tert*-butyl ester (6.10 g, 9.48 mmol) in DCM (50 mL) was cooled to 0 °C, and TFA (15 mL) was added slowly. After 20 min, the ice bath was removed and the contents allowed to reach room temperature. After 2 h at that temperature, the solvent was removed under reduced pressure. The residue was taken up in water (250 mL) and acetonitrile (25 mL) and stirred. Aqueous NH_4OH (28%) was then added until pH 9. The slurry was stirred for 15 min before the solid was collected and filtered. The solid was slurried a second time in dilute aqueous NH_4OH and the solid collected by filtration. The solid was then dried to give the title compound **33n** (3.87 g, 92%). MS (ESI) *m*/*z* 444.1 (M + 1); ^{1}H NMR (400 MHz, DMSO-d_6) δ 12.13 (br. S., 1 H), 10.55 (s, 1 H), 8.40 (s, 1 H), 8.29 (d, *J* = 8.8 Hz, 1 H), 8.16 (d, *J* = 3.5 Hz, 1 H), 7.40 (d, *J* = 2.3 Hz, 1 H), 7.08 (dd, *J* = 9.1, 2.3 Hz, 1 H), 6.70 (d, *J* = 3.8 Hz, 1 H), 6.30 (s, 1 H), 3.76−3.98 (m, 2 H), 2.92−3.05 (m, 1 H), 2.85 (dd, *J* = 16.5, 3.4 Hz, 1 H), 2.27−2.40 (m, 1 H), 1.41 (s, 3 H), 1.22 (d, *J* = 6.3 Hz, 3 H), 0.89−0.97 (m, 2 H), 0.73−0.82 (m, 2 H).

5-(6-Hydroxymethyl-pyrimidin-4-yloxy)-indole-1-carboxylic Acid (3-Trifluoromethyl-phenyl)-amide (***5a***). MS (ESI) *m*/*z* 429.1 (M + 1); ^{1}H NMR (400 MHz, methanol-d_4) δ 8.61 (d, *J* = 1.01 Hz, 1 H), 8.37 (d, *J* = 8.84 Hz, 1 H), 8.07 (s, 1 H), 7.96 (d, *J* = 3.79 Hz, 1 H), 7.90 (dd, *J* = 7.96, 1.39 Hz, 1 H), 7.58 (t, *J* = 7.96 Hz, 1 H), 7.45 (s, 1 H), 7.43 (d, *J* = 2.27 Hz, 1 H), 7.13 (dd, *J* = 8.97, 2.40 Hz, 1 H), 7.08 (d, *J* = 1.01 Hz, 1 H), 6.76 (d, *J* = 3.79 Hz, 1 H), 4.63 (s, 2 H).

5-((6-((Methylamino)methyl)pyrimidin-4-yl)oxy)-N-(3-(trifluoromethyl)phenyl)-1H-indole-1-carboxamide (***6a***). MS (ESI) *m*/*z* 442.1 (M + 1); ^{1}H NMR (400 MHz, methanol-d_4) δ 8.64 (s, 1 H), 8.34 (d, *J* = 9.09 Hz, 1 H), 8.05 (s, 1 H), 7.93 (d, *J* = 3.79 Hz, 1 H), 7.89 (d, *J* = 8.08 Hz, 1 H), 7.56 (t, *J* = 7.96 Hz, 1 H), 7.40−7.46 (m, 2 H), 7.10 (dd, *J* = 8.97, 2.40 Hz, 1 H), 6.99 (s, 1 H), 6.73 (d, *J* = 3.79 Hz, 1 H), 3.77 (s, 2 H), 2.40 (s, 3 H).

N-(4-Fluoro-3-(trifluoromethyl)phenyl)-5-((6-((methylamino)-methyl)pyrimidin-4-yl)oxy)-1H-indole-1-carboxamide (***6b***). MS (ESI) *m*/*z* 460.1 (M + 1); ^{1}H NMR (400 MHz, methanol-d_4) δ 8.65 (d, *J* = 1.01 Hz, 1 H), 8.35 (d, *J* = 8.84 Hz, 1 H), 8.04 (dd, *J* = 6.19, 2.65 Hz, 1 H), 7.90−7.94 (m, 2 H), 7.41 (d, *J* = 2.27 Hz, 1 H), 7.35 (t, *J* = 9.60 Hz, 1 H), 7.11 (dd, *J* = 8.97, 2.40 Hz, 1 H), 7.00 (s, 1 H), 6.74 (d, *J* = 3.79 Hz, 1 H), 3.82 (s, 2 H), 2.43 (s, 3 H).

5-((5,6,7,8-Tetrahydropyrido[3,4-d]pyrimidin-4-yl)oxy)-N-(3-(trifluoromethyl)phenyl)-1H-indole-1-carboxamide (***33a***). MS (ESI) *m*/*z* 454.0 (M + 1); ^{1}H NMR (400 MHz, DMSO-d_6) δ 10.43 (s, 1 H), 8.54 (s, 1 H), 8.30 (d, *J* = 8.8 Hz, 1 H), 8.15 (d, *J* = 3.5 Hz, 1 H), 8.11 (s, 1 H), 7.98 (d, *J* = 8.3 Hz, 1 H), 7.65 (t, *J* = 8.0 Hz, 1 H), 7.44−7.53 (m, 2 H), 7.14 (dd, *J* = 9.0, 2.4 Hz, 1 H), 6.81 (d, *J* = 3.8 Hz, 1 H), 4.26 (s, 2 H), 3.45 (t, *J* = 5.9 Hz, 2 H), 3.00 (t, *J* = 5.8 Hz, 2 H).

5-((5,6,7,8-Tetrahydropyrido[4,3-d]pyrimidin-4-yl)oxy)-N-(3-(trifluoromethyl)phenyl)-1H-indole-1-carboxamide (***33b***). MS (ESI) *m*/*z* 454.0 (M + 1); ^{1}H NMR (400 MHz, DMSO-d_6) δ 10.38 (s, 1 H), 8.46 (s, 1 H), 8.27 (d, *J* = 9.1 Hz, 1 H), 8.12 (d, *J* = 3.8 Hz, 1 H), 8.10 (s, 1 H), 7.97 (d, *J* = 8.1 Hz, 1 H), 7.65 (t, *J* = 8.0 Hz, 1 H), 7.50 (d, *J* = 7.3 Hz, 1 H), 7.46 (s, 1 H), 7.12 (dd, *J* = 9.0, 2.4 Hz, 1 H), 6.80 (d, *J* = 3.5 Hz, 1 H), 3.92−4.09 (m, 2 H), 3.17 (t, *J* = 5.7 Hz, 2 H), 2.81 (t, *J* = 5.7 Hz, 2 H).

(S)-5-((6-Methyl-5,6,7,8-tetrahydropyrido[3,4-d]pyrimidin-4-yl)-oxy)-N-(3-(trifluoromethyl)phenyl)-1H-indole-1-carboxamide (***33c***). MS (ESI) *m*/*z* 468.2 (M + 1); ^{1}H NMR (400 MHz, methanol-d_4) δ 8.37 (s, 1 H) 8.32 (d, *J* = 8.84 Hz, 1 H) 8.05 (s, 1 H) 7.92 (d, *J* = 3.79 Hz, 1 H) 7.89 (d, *J* = 8.59 Hz, 1 H) 7.56 (t, *J* = 7.96 Hz, 1 H) 7.44 (d, *J* = 7.83 Hz, 1 H) 7.39 (d, *J* = 2.27 Hz, 1 H) 7.09 (dd, *J* = 8.97, 2.40 Hz, 1 H) 6.73 (d, *J* = 3.79 Hz, 1 H) 3.89−4.09 (m, 2 H) 3.05−3.16 (m, 1 H) 2.99 (dd, *J* = 17.18, 3.79 Hz, 1 H) 2.47 (dd, *J* = 17.18, 10.36 Hz, 1 H) 1.34 (d, *J* = 6.57 Hz, 3 H).

(R)-5-((6-Methyl-5,6,7,8-tetrahydropyrido[3,4-d]pyrimidin-4-yl)-oxy)-N-(3-(trifluoromethyl)phenyl)-1H-indole-1-carboxamide (***33d***). MS (ESI) *m*/*z* 468.2 (M + 1); ^{1}H NMR (400 MHz, methanol-d_4) δ 8.37 (s, 1 H) 8.32 (d, *J* = 8.84 Hz, 1 H) 8.05 (s, 1 H) 7.92 (d, *J* = 3.79 Hz, 1 H) 7.89 (d, *J* = 8.59 Hz, 1 H) 7.56 (t, *J* = 7.96 Hz, 1 H) 7.44 (d, *J* = 7.83 Hz, 1 H) 7.39 (d, *J* = 2.27 Hz, 1 H) 7.09 (dd, *J* = 8.97, 2.40 Hz, 1 H) 6.73 (d, *J* = 3.79 Hz, 1 H) 3.89−4.09 (m, 2 H) 3.05−3.16 (m, 1 H) 2.99 (dd, *J* = 17.18, 3.79 Hz, 1 H) 2.47 (dd, *J* = 17.18, 10.36 Hz, 1 H) 1.34 (d, *J* = 6.57 Hz, 3 H).

5-((7-Acetyl-5,6,7,8-tetrahydropyrido[3,4-d]pyrimidin-4-yl)oxy)-N-(3-(trifluoromethyl)phenyl)-1H-indole-1-carboxamide (***33e***). MS (ESI) *m*/*z* 496.0 (M + 1); ^{1}H NMR (400 MHz, DMSO-d_6) δ 10.38 (s, 1 H), 8.45−8.53 (m, 1 H), 8.27 (d, *J* = 9.1 Hz, 1 H), 8.12 (d, *J* = 3.8 Hz, 1 H), 8.10 (s, 1 H), 7.97 (d, *J* = 8.8 Hz, 1 H), 7.65 (t, *J* = 8.1 Hz, 1 H), 7.50 (d, *J* = 7.8 Hz, 1 H), 7.47 (d, *J* = 2.3 Hz, 1 H), 7.14 (dd, *J* = 9.0, 2.4 Hz, 1 H), 6.80 (d, *J* = 3.5 Hz, 1 H), 4.63 (s, 2 H), 3.81 (t, *J* = 5.9 Hz, 2 H), 2.93 (t, *J* = 5.7 Hz, 2 H), 2.16 (s, 3 H).

5-((7-Ethyl-5,6,7,8-tetrahydropyrido[3,4-d]pyrimidin-4-yl)oxy)-N-(3-(trifluoromethyl)phenyl)-1H-indole-1-carboxamide (***33f***). MS (ESI) *m*/*z* 482.2 (M + 1); ^{1}H NMR (400 MHz, DMSO-d_6) δ 10.38 (br. S., 1 H), 8.42 (s, 1 H), 8.28 (d, *J* = 9.1 Hz, 1 H), 8.11 (d, *J* = 3.8 Hz, 1 H), 8.10 (s, 1 H), 7.96 (d, *J* = 9.1 Hz, 1 H), 7.63 (t, *J* = 8.0 Hz, 1 H), 7.48 (d, *J* = 7.8 Hz, 1 H), 7.46 (d, *J* = 2.5 Hz, 1 H), 7.13 (dd, *J* = 9.0, 2.4 Hz, 1 H), 6.78 (d, *J* = 3.8 Hz, 1 H), 3.57 (s, 2 H), 2.74−2.87 (m, 4 H), 2.59 (q, *J* = 7.2 Hz, 2 H), 1.12 (t, *J* = 7.2 Hz, 3 H).

5-((6,7-Dihydro-5H-pyrrolo[3,4-d]pyrimidin-4-yl)oxy)-N-(3-(trifluoromethyl)phenyl)-1H-indole-1-carboxamide (***33g***). MS (ESI) *m*/*z* 440.9 (M + 1); ^{1}H NMR (400 MHz, methanol-d_4) δ 8.55 (s, 1 H) 8.33 (d, *J* = 8.84 Hz, 1 H) 8.06 (br. S., 1 H) 7.89 (d, *J* = 8.34 Hz, 1 H) 7.94 (d, *J* = 3.54 Hz, 1 H) 7.57 (t, *J* = 7.96 Hz, 1 H) 7.41−7.46 (m, 2 H) 7.13 (dd, *J* = 9.09, 2.27 Hz, 1 H) 6.74 (d, *J* = 3.03 Hz, 1 H) 4.26 (d, *J* = 12.13 Hz, 4 H).

(S)-5-(5-Methyl-6,7-dihydro-5H-pyrrolo[3,4-d]pyrimidin-4-yloxy)-indole-1-carboxylic Acid (3-trifluoromethyl-phenyl)-amide (***33h***). MS (ESI) *m*/*z* 454.9 (M + 1); ^{1}H NMR (400 MHz, methanol-d_4) δ 8.47 (d, *J* = 1.77 Hz, 1 H) 8.28 (dd, *J* = 9.09, 1.77 Hz, 1 H) 8.02 (s, 1 H) 7.85 (dd, *J* = 3.66, 2.40 Hz, 2 H) 7.49 (t, *J* = 7.83 Hz, 1 H) 7.36 (d, *J* = 2.02 Hz, 1 H) 7.38 (d, *J* = 8.59 Hz, 1 H) 7.06 (dd, *J* = 8.84, 2.27 Hz, 1 H) 6.65 (d, *J* = 2.53 Hz, 1 H) 4.63 (d, *J* = 6.06 Hz, 1 H) 4.15−4.23 (m, 1 H) 4.05−4.12 (m, 1 H) 1.55 (d, *J* = 6.57 Hz, 3 H).

(R)-5-(5-Methyl-6,7-dihydro-5H-pyrrolo[3,4-d]pyrimidin-4-yloxy)-indole-1-carboxylic Acid (3-trifluoromethyl-phenyl)-amide (***33i***). MS (ESI) *m*/*z* 454.9 (M + 1); ^{1}H NMR (400 MHz, methanol-d_4) δ 8.48 (s, 1 H) 8.30 (d, *J* = 9.09 Hz, 1 H) 8.03 (s, 1 H) 7.87 (d, *J* = 3.54 Hz, 2 H) 7.52 (t, *J* = 8.08 Hz, 1 H) 7.38 (d, *J* = 2.27 Hz, 2 H) 7.07 (dd, *J* = 8.84, 2.27 Hz, 1 H) 6.67 (d, *J* = 3.79 Hz, 1 H) 4.66 (q, *J* = 6.57 Hz, 1 H) 4.12−4.22 (m, 2 H) 1.56 (d, *J* = 6.57 Hz, 3 H).

5-(5,6,7,8-Tetrahydro-pyrido[3,4-d]pyrimidin-4-yloxy)-indole-1-carboxylic Acid (5-Methyl-pyridin-3-yl)-amide (***33j***). MS (ESI) *m*/*z* 401.1 (M + 1); ^{1}H NMR (methanol-d_4) δ 8.64 (d, *J* = 2.0 Hz, 1 H), 8.37 (s, 1 H), 8.33 (d, *J* = 8.8 Hz, 1 H), 8.18 (d, *J* = 1.0 Hz, 1 H), 8.03 (s, 1 H), 7.92 (d, *J* = 3.5 Hz, 1 H), 7.40 (d, *J* = 2.3 Hz, 1 H), 7.10 (dd, *J* = 9.1, 2.3 Hz, 1 H), 6.74 (d, *J* = 3.0 Hz, 1 H), 3.95 (s, 2 H), 3.18 (t, *J* = 5.9 Hz, 2 H), 2.88 (t, *J* = 5.8 Hz, 2 H), 2.41 (s, 3 H).

5-(5,6,7,8-Tetrahydro-pyrido[3,4-d]pyrimidin-4-yloxy)-indole-1-carboxylic Acid (5-Isopropyl-1H-pyrazol-3-yl)-amide (***33k***). MS (ESI) *m*/*z* 418.2 (M + 1); ^{1}H NMR (DMSO-d_6) δ 12.21 (br. S., 1 H), 10.56 (s, 1 H), 8.39 (s, 1 H), 8.29 (d, *J* = 9.1 Hz, 1 H), 8.16 (d, *J* = 3.5 Hz, 1 H), 7.41 (d, *J* = 2.3 Hz, 1 H), 7.08 (dd, *J* = 9.1, 2.3 Hz, 1 H), 6.70 (d, *J* = 3.5 Hz, 1 H), 6.34 (s, 1 H), 3.81 (s, 2 H), 2.87−3.07 (m, 3 H), 2.72 (t, *J* = 5.6 Hz, 2 H), 1.25 (d, *J* = 6.8 Hz, 6 H).

DOI: 10.1021/acs.jmedchem.5b01227
J. Med. Chem. 2015, 58, 9273−9286

*5-(5,6,7,8-Tetrahydro-pyrido[3,4-d]pyrimidin-4-yloxy)-indole-1-carboxylic Acid (5-tert-Butyl-2H-pyrazol-3-yl)-amide (**33l**).* MS (ESI) m/z 432.1 (M + 1); ^{1}H NMR (methanol-d_4) δ 8.37 (s, 1 H), 8.32 (d, J = 8.8 Hz, 1 H), 7.88 (d, J = 3.5 Hz, 1 H), 7.38 (d, J = 2.3 Hz, 1 H), 7.08 (dd, J = 9.1, 2.3 Hz, 1 H), 6.71 (d, J = 3.8 Hz, 1 H), 6.37 (s, 1 H), 3.96 (s, 2 H), 3.19 (t, J = 5.9 Hz, 2 H), 2.89 (t, J = 5.7 Hz, 2 H), 1.36 (s, 9 H).

*5-(5,6,7,8-Tetrahydro-pyrido[3,4-d]pyrimidin-4-yloxy)-indole-1-carboxylic Acid [5-(1-Methyl-cyclopropyl)-2H-pyrazol-3-yl]-amide (**33m**).* HRMS (ESI+) m/z calculated for $C_{23}H_{23}N_7O_2$ (M + 1) 430.1993, found 430.1992; ^{1}H NMR (DMSO-d_6) δ 12.13 (br. S., 1 H), 10.55 (s, 1 H), 8.40 (s, 1 H), 8.29 (d, J = 8.8 Hz, 1 H), 8.16 (d, J = 3.8 Hz, 1 H), 7.41 (d, J = 2.3 Hz, 1 H), 7.08 (dd, J = 9.0, 2.4 Hz, 1 H), 6.70 (d, J = 3.5 Hz, 1 H), 6.29 (s, 1 H), 3.84 (s, 2 H), 3.05 (t, J = 5.8 Hz, 2 H), 2.69−2.78 (m, 2 H), 1.41 (s, 3 H), 1.25 (br. S., 2 H), 0.89−0.97 (m, 2 H); ^{13}C NMR (400 MHz, DMSO-d_6) δ 166.9, 165.7, 154.3, 149.1, 148.7, 147.5, 146.5, 132.9, 130.2, 126.4, 118.0, 115.7, 115.4, 113.2, 106.2, 93.8, 49.4, 41.9, 22.6, 22.0, 15.6, 12.6.

*5-((S)-6-Methyl-5,6,7,8-tetrahydro-pyrido[3,4-d]pyrimidin-4-yloxy)-indole-1-carboxylic Acid [5-(1-Methyl-cyclopropyl)-2H-pyrazol-3-yl]-amide (**33n**).* HRMS (ESI+) m/z calculated for $C_{24}H_{25}N_7O_2$ (M + 1) 444.2149, found 444.2143; ^{1}H NMR (400 MHz, DMSO-d_6) δ 12.13 (br. S., 1 H), 10.55 (s, 1 H), 8.40 (s, 1 H), 8.29 (d, J = 8.8 Hz, 1 H), 8.16 (d, J = 3.5 Hz, 1 H), 7.40 (d, J = 2.3 Hz, 1 H), 7.08 (dd, J = 9.1, 2.3 Hz, 1 H), 6.70 (d, J = 3.8 Hz, 1 H), 6.30 (s, 1 H), 3.76−3.98 (m, 2 H), 2.92−3.05 (m, 1 H), 2.85 (dd, J = 16.5, 3.4 Hz, 1 H), 2.27−2.40 (m, 1 H), 1.41 (s, 3 H), 1.22 (d, J = 6.3 Hz, 3 H), 0.89−0.97 (m, 2 H), 0.73−0.82 (m, 2 H); ^{13}C NMR (400 MHz, DMSO-d_6) δ 166.8, 165.1, 154.4, 149.1, 148.7, 147.5, 146.5, 132.9, 130.2, 126.4, 118.0, 115.7, 115.1, 113.2, 106.3, 93.8, 49.4, 47.7, 29.6, 22.6, 21.5, 15.6, 12.6.

*5-(6,7-Dihydro-5H-pyrrolo[3,4 d]pyrimidin-4-yloxy)-indole-1-carboxylic Acid [5-(1-methyl-cyclopropyl)-2H-pyrazol-3-yl]-amide (**33o**).* MS (ESI) m/z 416.2 (M + 1); ^{1}H NMR (400 MHz, DMSO-d_6) δ 12.13 (s, 1H) 10.57 (s, 1 H) 8.55 (s, 1 H) 8.29 (d, J = 9.09 Hz, 1 H) 8.17 (d, J = 3.79 Hz, 1 H) 7.44 (d, J = 2.27 Hz, 1 H) 7.11 (dd, J = 9.09, 2.53 Hz, 1 H) 6.71 (d, J = 3.54 Hz, 1 H) 6.29 (s, 1 H) 4.09 (d, J = 12.63 Hz, 4 H) 1.41 (s, 3 H) 0.91−0.93 (m, 2 H) 0.74−0.78 (m, 2 H).

*5-(R)-6-Methyl-5,6,7,8-tetrahydro-pyrido[3,4-d]pyrimidin-4-yloxy)-indole-1-carboxylic Acid [5-(1-methyl-cyclopropyl)-2H-pyrazol-3-yl]-amide (**33p**).* MS (ESI) m/z 444.1 (M + 1); ^{1}H NMR (400 MHz, methanol-d_4) δ 8.51 (s, 1 H), 8.34 (d, J = 9.0 Hz, 1 H), 7.90 (d, J = 3.8 Hz, 1 H), 7.41 (d, J = 2.1 Hz, 1 H), 7.10 (dd, J = 9.0, 2.3 Hz, 1 H), 6.72 (d, J = 3.7 Hz, 1 H), 6.28 (s, 1 H), 3.73−3.88 (m, 1 H), 2.86 (dd, J = 17.9, 10.7 Hz, 1 H), 1.59 (d, J = 6.4 Hz, 3 H), 1.46 (s, 3 H), 0.92−1.03 (m, 2 H), 0.75−0.88 (m, 2 H).

*5-(5,6,7,8-Tetrahydro-pyrido[3,4-d]pyrimidin-4-yloxy)-indole-1-carboxylic Acid (5-tert-Butyl-isoxazol-3-yl)-amide (**33q**).* MS (ESI) m/z 432.9 (M + 1); ^{1}H NMR (400 MHz, methanol-d_4) δ 8.37 (s, 1 H) 8.33 (d, J = 8.84 Hz, 1 H) 7.88 (d, J = 3.79 Hz, 1 H) 7.38 (d, J = 2.02 Hz, 1 H) 7.10 (dd, J = 8.84, 2.27 Hz, 1 H) 6.72 (d, J = 3.79 Hz, 1 H) 6.65 (s, 1 H) 3.94 (s, 2 H) 3.17 (t, J = 5.94 Hz, 2 H) 2.87 (t, J = 5.68 Hz, 2 H) 1.38 (s, 9 H).

*5-((S)-6-Methyl-5,6,7,8-tetrahydro-pyrido[3,4-d]pyrimidin-4-yloxy)-indole-1-carboxylic Acid (5-tert-Butyl-isoxazol-3-yl)-amide (**33r**).* MS (ESI) m/z 447.2 (M + 1); ^{1}H NMR (400 MHz, DMSO-d_6) δ 8.40 (s, 1 H) 8.29 (d, J = 9.09 Hz, 1 H) 8.15 (d, J = 3.28 Hz, 1 H) 7.43 (d, J = 1.26 Hz, 1 H) 7.11 (dd, J = 8.72, 1.39 Hz, 1 H) 6.75 (d, J = 3.03 Hz, 1 H) 6.68 (s, 1 H) 3.79−3.98 (m, 2 H) 2.91−3.05 (m, 1 H) 2.85 (d, J = 16.17 Hz, 1 H) 2.34 (dd, J = 16.17, 9.60 Hz, 1 H) 1.34 (s, 9 H) 1.21 (d, J = 6.32 Hz, 3 H).

*5-(6,7-Dihydro-5H-pyrrolo[3,4-d]pyrimidin-4-yloxy)-indole-1-carboxylic Acid (5-tert-Butyl-isoxazol-3-yl)-amide (**33s**).* MS (ESI) m/z 419.2 (M + 1); ^{1}H NMR (400 MHz, DMSO-d_6) δ 8.56 (s, 1 H) 8.29 (d, J = 8.84 Hz, 1 H) 8.17 (d, J = 3.79 Hz, 1 H) 7.47 (d, J = 2.27 Hz, 1 H) 7.15 (dd, J = 8.97, 2.40 Hz, 1 H) 6.76 (d, J = 3.28 Hz, 1 H) 6.68 (s, 1 H) 4.07−4.14 (m, 4 H) 1.34 (s, 9 H).

*6,7-Dihydro-5H-pyrrolo[3,4-d] pyrimidin-4-yloxy)-indole-1-carboxylic acid (3-tert-butyl-isoxazol-5-yl)-amide (**33t**).* MS (ESI) m/z 419.9 (M + 1); ^{1}H NMR (400 MHz, DMSO-d_6) δ 8.61 (s, 1 H) 8.42 (d, J = 9.09 Hz, 1 H) 8.11 (d, J = 3.79 Hz, 1 H) 7.44 (d, J = 2.27 Hz, 1 H) 7.11 (dd, J = 9.22, 2.40 Hz, 1 H) 6.67 (d, J = 3.54 Hz, 1 H) 6.22 (s, 1 H) 4.25 (br. S., 4 H) 1.28 (s, 9 H).

*(S)-5-(Methyl-6,7-dihydro-5H-pyrrolo[3,4-d]pyrimidin-4-yloxy)-indole-1-carboxylic Acid (5-tert-Butyl-isoxazol-3-yl)-amide (**33u**).* MS (ESI) m/z 433.0 (M + 1); ^{1}H NMR (400 MHz, DMSO-d_6) δ 8.54 (s, 1 H) 8.30 (d, J = 9.09 Hz, 1 H) 8.16 (d, J = 3.79 Hz, 1 H) 7.46 (d, J = 2.27 Hz, 1 H) 7.14 (dd, J = 8.97, 2.40 Hz, 1 H) 6.76 (d, J = 3.79 Hz, 1 H) 6.68 (s, 1 H) 4.62 (d, J = 6.57 Hz, 1 H) 4.12 (d, J = 2.27 Hz, 1 H) 4.08 (d, J = 1.52 Hz, 1 H) 1.44 (d, J = 6.57 Hz, 3 H) 1.34 (s, 9 H).

*5-(6,7-Dihydro-5H-pyrrolo[3,4-d] pyrimidin-4-yloxy)-indole-1-carboxylic Acid (5-Cyclopropyl-isoxazol-3-yl)-amide (**33v**).* HRMS (ESI+) m/z calculated for $C_{21}H_{18}N_6O_3$ (M + 1) 403.1520, found 403.1520; ^{1}H NMR (400 MHz, DMSO-d_6) δ 8.55 (s, 1 H) 8.29 (d, J = 9.09 Hz, 1 H) 8.16 (d, J = 3.79 Hz, 1 H) 7.46 (d, J = 2.27 Hz, 1 H) 7.14 (dd, J = 8.97, 2.40 Hz, 1 H) 6.75 (d, J = 3.28 Hz, 1 H) 6.65 (s, 1 H) 4.04−4.16 (m, 4 H) 2.07−2.26 (m, 1 H) 1.01−1.15 (m, 2 H) 0.87−0.98 (m, 2 H); ^{13}C NMR (400 MHz, DMSO-d_6) δ 175.2, 174.6, 164.4, 158.7, 157.3, 149.1, 147.7, 133.1, 130.6, 126.7, 118.5, 118.4, 116.0, 113.5, 107.2, 93.9, 52.8, 487.9, 8.2, 8.0.

*5-(6,7-Dihydro-5H-pyrrolo[3,4-d] pyrimidin-4-yloxy)-indole-1-carboxylic Acid (5-Isopropyl-isoxazol-3-yl)-amide (**33w**).* MS (ESI) m/z 405.1 (M + 1); ^{1}H NMR (400 MHz, DMSO-d_6) δ 8.56 (s, 1 H) 8.29 (d, J = 8.84 Hz, 1 H) 8.17 (d, J = 3.79 Hz, 1H) 7.47 (d, J = 2.27 Hz, 1 H) 7.15 (dd, J = 8.97, 2.40 Hz, 1 H) 6.76 (d, J = 3.79 Hz, 1 H) 6.69 (s, 1 H) 4.00−4.20 (m, 4 H) 3.11 (m, 1 H) 1.29 (d, J = 7.07 Hz, 6 H).

*5-(6,7-Dihydro-5H-pyrrolo[3,4-d] pyrimidin-4-yloxy)-indole-1-carboxylic Acid [5-(1-Methyl-cyclopropyl)-isoxazol-3-yl]-amide (**33x**).* MS (ESI) m/z 417.1 (M + 1); ^{1}H NMR (400 MHz, DMSO-d_6) δ 8.56 (s, 1 H) 8.29 (d, J = 8.84 Hz, 1 H) 8.16 (d, J = 3.79 Hz, 1 H) 7.47 (d, J = 2.53 Hz, 1 H) 7.15 (dd, J = 8.97, 2.40 Hz, 1 H) 6.76 (d, J = 3.28 Hz, 1 H) 6.67 (s, 1 H) 4.01−4.19 (m, 4 H + 1 N−H) 1.46 (s, 3 H) 1.07−1.21 (m, 2 H) 0.86−1.02 (m, 2 H).

Mouse Laser-Induced Choroidal Neovascularization (CNV) Model. The animal research presented in this article was approved by the Novartis Institutes for Biomedical Research IACUC Committee. We used female C57/BL6 mice that were typically 8−10 weeks old. Mice used in an experiment arrived at our research facility in a single shipment. Experimental interventions for a cohort of animals were started on the same day. Mice were treated by oral gavage with compound starting 1 h before laser treatment (Day 0) and continuing once a day through Day 6 after laser treatment. Experimental groups were dosed with either vehicle (0.5% methylcellulose and 0.2% Tween 80) or compound in vehicle (0.5% methylcellulose and 0.2% Tween 80) at 10 mg/kg. Each group consisted of 10 mice, with 3 laser burns to each eye yielding 60 data per group.

Laser Photocoagulation. Mouse pupils were dilated with one drop (volume 40 μL) of 1% cyclopentolate. Just before anesthesia, pupil dilation was maximized with an additional drop of phenylephrine (usually 10% but occasionally 2.5% depending upon availability). Mice were then anaesthetized with an intraperitoneal (i.p.) injection of a mixture of ketamine and xylazine at doses up to100 mg/kg and 10 mg/kg, respectively. Prior to laser pulse application, each eye was anesthetized with topical 0.5% proparacaine. Lubricating eyedrops (Genteals Novartis) on a glass coverslip were applied to the cornea, and the retina was viewed through a slit lamp microscope. Three laser pulses were applied to the fundus around the optic nerve of each eye, six laser pulses in total for each mouse. The pulses were from a green laser (wavelength = 532 nm; Oculight GLx) and had a duration of 30 ms, a power of 120 mW, and a spot size of 100 μm. A successful laser burn generated a yellow vaporization bubble which correlated with a rupture of Bruch's membrane. If a vaporization bubble did not form, one additional laser pulse would be administered to the same spot. For each eye, a maximum of four shots were allowed. An additional fourth shot was required in fewer than 3% of eyes. After the application of laser burns to both eyes, antibiotic ointment (0.5% Erythromycin, Tobramycin, or Neomycin ophthalmic ointment depending on availability and cost) was applied to both eyes.

Harvest and Photography of CNV Lesions. Unless indicated, studies were completed 7 days after laser photocoagulation. On the

DOI: 10.1021/acs.jmedchem.5b01227
J. Med. Chem. 2015, 58, 9273−9286

final study day, 0.1 mL of a 5 mg/mL solution of FITC concanavalin-A (Vector Laboratories) was injected intravenously (i.v.) to fluorescently label the vascular endothelium. Animals were sacrificed 15−30 min later with inhaled carbon dioxide. Eyes were enucleated and fixed in 4% paraformaldehyde for approximately 60 min at room temperature and then transferred to vials of PBS. Posterior eye cups were dissected from the eyes. The RPE-choroidal-sclera complexes were separated from the neural retina and mounted on microscope slides, at which time each eye was given a randomization code to mask the examiners. Fluorescent images of each CNV lesion were photographed with an Axiocam MR3 camera on an Axio Image M1 microscope (Zeiss). CNV area was quantified using a semiautomated analysis program (Axiovision software, version 4.5, Zeiss) that outlined the fluorescent blood vessels. Image capture, CNV area measurement, and exclusions (see below) were performed on masked microscope slides.

Measurements of Neovascular Lesions. Most eyes generated three data points corresponding to the area of each of the three laser-induced CNV lesions. A cohort of 10 mice with both eyes treated would optimally provide 60 data points. However, a lesion would be necessarily excluded for any of the following reasons: (1) there was choroidal hemorrhage encroaching on the lesion; (2) the lesion was of irregular shape indicating an asymmetrical laser burn; (3) the lesion had fused with another lesion; (4) the lesion had a size indicating that it was an outlier lesion, as defined below; or (5) the lesion was the only lesion in an eye (i.e., if 2 of the 3 lesions in an eye were excluded, then all lesions in that eye were excluded).

An outlier lesion fell into one of the following three categories: (1) "too big", i.e., it was over 10,000 μ^2 in area, and it was more than 5 times larger than the next biggest lesions in the eye (for reference, the mean area of CNV in a control group typically ranged from 10,000 to 20,000 μ^2); (2) "too small", i.e., it was less than 1/5 the area of the other next smallest lesion in the eye; this criterion applied only if at least one lesion in the eye was over 5,000 μ^2; (3) "too different", i.e., after all of the lesions in a specific treatment group were measured, the lesion's area was 5-fold greater than the mean for that group; this criterion applied only for lesions that were ≥5,000 μ^2.

Other reasons that lesions were excluded or not measured include: (1) the death of a mouse before the end of an experiment; (2) the failure of the i.v. injection of the vascular label; (3) the laser could not be applied due to media opacities (e.g., a pre-existing corneal scar or cataract); in this case, the fellow eye could still be included; (4) there was damage to the CNV lesion during tissue processing (if any part of the CNV was cut or not discernible, it was not included); and (5) a CNV lesion could not be located during the imaging of an eyecup.

Rat Laser-Induced Choroidal Neovascularization (CNV) Model. We used male Brown Norway rats that were typically 12 weeks old (range of age 7−14 weeks). Rats were purchased from Harlan, and the rats used in a single experiment arrived at our research facility in a single shipment and were age-matched. Experimental interventions for a cohort of animals were started on the same day. Laser application for an individual experiment was by a single scientist. Cages were randomly assigned to treatment groups with rats sharing a cage receiving the same treatment.

Laser Photocoagulation. Rat pupils were dilated with one drop (volume ∼40 μL) of 1% cyclopentolate. Just before anesthesia, pupil dilation was maximized with an additional drop of phenylephrine (usually 10% but occasionally 2.5% depending upon availability). Rats were then anaesthetized with an intraperitoneal (i.p.) injection of a mixture of ketamine and xylazine at doses of 40−80 mg/kg and 5−10 mg/kg, respectively. Prior to laser pulse application, each eye was anesthetized with topical 0.5% proparacaine. Lubricating eyedrops (Genteal Alcon Laboratories, Fort Worth, TX) on a glass coverslip were applied to the cornea, and the retina was viewed through a slit lamp microscope. Each laser pulse was applied approximately 1 mm from the optic nerve; single pulses in each of four separate locations were applied to each eye for a total of eight laser photocoagulation sites for each mouse. The pulses were from a green laser (wavelength = 532 nm; Oculight GLx Mountain View, CA) and had a duration of 30 ms, a power of 190 mW, and a spot size of 200 μm. A successful laser pulse generated a yellow vaporization bubble which correlated with a rupture of Bruch's membrane (evaluated histologically in control rats sacrificed 6 h after lasering; data not shown). In cases when a vaporization bubble did not form (<1% of laser pulses), one additional laser pulse could be administered to the same spot. For each eye, a maximum of five laser pulses were allowed to generate 4 lesions. After the application of laser burns to both eyes, antibiotic ointment (Tobramycin or Neomycin ophthalmic ointment depending on availability and cost) was applied to both eyes.

Tissue Processing, Imaging, and CNV Area Quantification. Analysis of neovascularization was completed on tissues harvested 11, 12, or 14 days after laser photocoagulation depending on the dosing paradigm of the experiment. For an individual experiment, all rats were euthanized on the same day after alser photocoagulation. On the final study day, 0.2 mL of a 12.5 mg/mL solution of a 2,000 kDa FITC dextran (Sigma) was injected intravenously (i.v.) to fluorescently label the vascular endothelium. Animals were euthanized 15−30 min later with inhaled carbon dioxide. Eyes were enucleated and fixed in 4% paraformaldehyde (Vector Laboratories, Burlingame, CA) for approximately 60 min at room temperature, and then, the fixative was replaced with PBS. Each eye was assigned a randomized number to mask the samples for the remainder of the analysis. Posterior segments were isolated, and retinas were removed. The posterior eye cups which included the retinal pigment epithelium (RPE), the choroid, and the sclera were flat-mounted onto microscope slides after making 3 or 4 radial cuts. Fluorescent images of each CNV lesion were photographed with an Axiocam MR3 camera on an Axio Image M1 microscope (Carl Zeiss Microscopy, Thornwood, NY). CNV area was quantified using a semiautomated analysis program (Axiovision software, version 4.5, Carl Zeiss Microscopy) that outlined the fluorescent blood vessels. Image capture, CNV area measurement, and exclusions (see below) were performed on randomized samples or data by scientists masked to the treatment group.

Compound Administration. Test articles were administered via oral gavage, starting approximately 1 h before lasering, unless described otherwise.

Application of Exclusion Criteria. Each eye typically generates 4 data points corresponding to the area of 4 individual CNV lesions. In a typical study, a cohort of 10 rats per group would optimally provide 80 data points. However, a lesion would be excluded for any of the following reasons: (1) there was choroidal hemorrhage encroaching on the lesion; (2) the lesion was linear instead of circular, a consequence of a deflected ("split") laser impact; (3) the lesion had fused with another lesion; (4) the lesion had a size indicating that it was an outlier lesion as defined below; or (5) the lesion was the only lesion in an eye (i.e., if 3 of the 4 lesions in an eye were excluded, then all lesions in that eye were excluded).

An outlier lesion fell into one of the following three categories: (1) "too big", i.e., it was over 10,000 μ^2 in area and was more than 5 times larger than the next biggest lesion in the eye (for reference, the mean area of CNV in a control group typically ranged from 10,000 to 20,000 μ^2); (2) "too small", i.e., it was less than 1/5 the area of the next smallest lesion in the eye; this criterion applied only if at least one lesion in the eye was over 5,000 μ^2; (3) "too different", i.e., after all of the lesions in a specific treatment group were measured, the lesion's area was 5-fold greater than the mean for that group; this criterion applied only for lesions that were ≥5,000 μ^2.

Other reasons that lesions were excluded or not measured include: (1) the death of a rat before the end of an experiment; (2) the failure of the i.v. injection of the vascular label; (3) media opacities precluding accurate laser application (e.g., a pre-existing corneal scar or cataract); in this case, the fellow eye could still be included; (4) damage to the CNV lesion during tissue processing (i.e., poor quality of the tissue during processing so that the lesion could not be fully delineated); (5) inability to locate a CNV lesion during the imaging of an eyecup.

Ocular PK in Brown Norway Rats Following Administration of a Single Oral Dose. Three month old Brown Norway rats were administered orally with an active agent as shown in Table 6 at the dosing concentration and formulation specified. Ocular tissues and plasma were collected from 2 rats per active agent at 6, 24, 48, 72, 96, 120, and 144 h after dosing. The ocular tissues collected were the

DOI: 10.1021/acs.jmedchem.5b01227
J. Med. Chem. 2015, 58, 9273−9286

retina and the posterior eye cup. Each time point had drug levels measured in 4 individual retinas, 4 individual posterior eye cups, and 2 individual plasma samples.

Ocular tissues were homogenized and plasma proteins precipitated, and the drug concentration was analyzed by LC-MS/MS. Exposures in the retina, posterior eye cup (PEC), and plasma for the compounds were dose normalized and are listed in Table 6 as area under the curve measurements (AUC), C_{max}, and $C_{24\ h}$.

AUTHOR INFORMATION

Corresponding Author

*E-mail: erik.meredith@novartis.com.

Present Addresses

[⊥]N.M.: Raze Therapeutics, 400 Technology Square, Cambridge, MA 02139.

[#]J.K.: Department of Ophthalmology and Vision Science, University of Toronto, and Department of Vision Sciences, Toronto Western Research Institute, 399 Bathurst Street, Toronto, Ontario M5T 2S8, Canada.

[▽]K.M.: My Health Partners, 39 Pleasant Blvd., Toronto, ON, M4T 1K2, Canada.

[○]L.J.: Coditas Group, 125 Westbourne Terrace, Brookline, MA 02446.

[◆]N. J.: Mitobridge, Inc., 1030 Massachusetts Avenue, Suite 200, Cambridge, MA 02138.

[¶]G.A.: Kalexsyn, 4502 Campus Drive, Kalamazoo, MI, 49008.

[+]L.H.: Sensirion, Laubisruetistrasse, 508712 Staefa ZH, Switzerland.

[×]V.H.: AstraZeneca Neuroscience Innovative Medicines, 141 Portland Street, 10th Floor, Cambridge, MA, 02139.

[∞]C.R.: School of Biological Science, Nanyang Technological University, 60 Nanyang Drive, Singapore, 637551.

[÷]Y.Z.: 4237 Time Square Blvd., Dublin, OH 43016.

Notes

The authors declare no competing financial interest.

ACKNOWLEDGMENTS

We acknowledge the contribution of the Novartis Institute for Biomedical Research Analytical Sciences group and the Novartis Institute for Biomedical Research Metabolism and Pharmacokinetics group for support in generating the analytical details for the compounds described herein.

ABBREVIATIONS USED

TLC, thin layer chromatography; VEGF, vascular endothelial growth factor; AMD, age-related macular degeneration; ADME, absorption distribution metabolism excretion; CNV, choroidal neovascularization; PEC, posterior eye cup; p.o., oral; i.v., intravenous; i.v.t., intravitreal; ETDRS, Early Treatment of Diabetic Retinopathy Study; WFI, water for injection; MC, methylcellulose; CMC, carboxymethylcellulose; DN, dose normalized

REFERENCES

(1) CATT Research Group. Ranibizumab and Bevacizumab for Neovascular Age-Related Macular Degeneration. *N. Engl. J. Med.* **2011**, *364*, 1897−1908.

(2) Brown, D. M.; Kaiser, P. K.; Michels, M.; Soubrane, G.; Heier, J. S.; Kim, R. Y.; Sy, J. P.; Schneider, S. Ranibizumab versus verteporfin for neovascular age-related macular degeneration. *N. Engl. J. Med.* **2006**, *355*, 1432−1444.

(3) Ferrara, N.; Davis-Smyth, T. The biology of vascular endothelial growth factor. *Endocr. Rev.* **1997**, *18* (1), 4−25.

(4) Bates, D. O.; Curry, F. E. Vascular endothelial growth factor increases microvascular permeability via a Ca^{2+}-dependent pathway. *Am. J. Physiol.* **1997**, *273* (2 Pt 2), H687−694.

(5) Gao, H.; Qiao, X.; Gao, R.; Mieler, W. F.; McPherson, A. R.; Holz, E. R. Intravitreal triamcinolone does not alter basal vascular endothelial growth factor mRNA expression in rat retina. *Vision Res.* **2004**, *44* (4), 349−356.

(6) Lopez, P. F.; Sippy, B. D.; Lambert, H. M.; Thach, A. B.; Hinton, D. R. Transdifferentiated retinal pigment epithelial cells are immunoreactive for vascular endothelial growth factor in surgically excised age-related macular degeneration-related choroidal neovascular membranes. *Invest. Ophthalmol. Vis. Sci.* **1996**, *37* (5), 855−868.

(7) Aiello, L. P.; Avery, R. L.; Arrigg, P. G.; Keyt, B. A.; Jampel, H. D.; Shah, S. T.; Pasquale, L. R.; Thieme, H.; Iwamoto, M. A.; Park, J. E.; Nguyen, H. V.; Aiello, L. M.; Ferrara, N.; King, G. L. Vascular endothelial growth factor in ocular fluid of patients with diabetic retinopathy and other retinal disorders. *N. Engl. J. Med.* **1994**, *331* (22), 1480−1487.

(8) Nguyen, Q. D.; Tatlipinar, S.; Shah, S. M.; Haller, J. A.; Quinlan, E.; Sung, J.; Zimmer-Galler, I.; Do, D. V.; Campochiaro, P. A. Vascular endothelial growth factor is a critical stimulus for diabetic macular edema. *Am. J. Ophthalmol.* **2006**, *142* (6), 961−9.

(9) Terman, B. I.; Dougher-Vermazen, M.; Carrion, M. E.; Dimitrov, D.; Armellino, D. C.; Gospodarowicz, D.; Böhlen, P. Identification of the KDR tyrosine kinase as a receptor for vascular endothelial cell growth factor. *Biochem. Biophys. Res. Commun.* **1992**, *187* (3), 1579−1586.

(10) Shalaby, F.; Rossant, J.; Yamaguchi, T. P.; Gertsenstein, M.; Wu, X. F.; Breitman, M. L.; Schuh, A. C. Failure of blood-island formation and vasculogenesis in Flk-1-deficient mice. *Nature* **1995**, *376* (6535), 62−66.

(11) Matsumoto, T.; Claesson-Welsh, L. VEGF receptor signal transduction. *Sci. Signaling* **2001**, *2001* (112), re21.

(12) Keefe, D.; Bowen, J.; Gibson, R.; Tan, T.; Okera, M.; Stringer, A. Noncardiac vascular toxicities of vascular endothelial growth factor inhibitors in advanced cancer: a review. *Oncologist* **2011**, *16* (4), 432−444.

(13) Boyer, S. J. Small molecule inhibitors of KDR (VEGFR-2)kinase: an overview of structure activity relationships. *Curr. Top. Med. Chem.* **2002**, *2*, 973−1000.

(14) Schenone, S.; Bondavalli, F.; Botta, M. Antiangiogenic agents: an update on small molecule VEGFR inhibitors. *Curr. Med. Chem.* **2007**, *14*, 2495−2516.

(15) Musumeci, F.; Radi, M.; Brullo, C.; Schenone, S. Vascular Endothelial Growth Factor (VEGF) Receptors: Drugs and New Inhibitors. *J. Med. Chem.* **2012**, *55*, 10797−10822 and references therein..

(16) Diago, T.; Pulido, J. S.; Molina, J. R.; Collett, L. C.; Link, T. P.; Ryan, E. H., Jr. Ranibizumab combined with low-dose sorafenib for exudative age-related macular degeneration. *Mayo Clin. Proc.* **2008**, *83*, 231−234.

(17) Kernt, M.; Staehler, M.; Stief, C.; Kampik, A.; Neubauer, A. S. Resolution of macular oedema in occult choroidal neovascularization under oral Sorafenib treatment. *Acta Ophthalmol.* **2008**, *86*, 456−458.

(18) Amparo, F.; Sadrai, Z.; Jin, Y.; Alfonso-Bartolozzi, B.; Wang, H.; Shikari, H.; Ciolino, J. B.; Chodosh, J.; Jurkunas, U.; Schaumberg, D. A.; Dana, R. Safety and Efficacy of the Multitargeted Receptor Kinase Inhibitor Pazopanib in the Treatment of Corneal Neovascularization. *Invest. Ophthalmol. Visual Sci.* **2013**, *54*, 537−544.

(19) Kwak, N.; Okamoto, N.; Wood, J. M.; Campochiaro, P. A. VEGF is major stimulator in model of choroidal neovascularization. *Invest. Ophthalmol. Vis. Sci.* **2000**, *41*, 3158−3164.

(20) Bold, G.; Capraro, H.-G.; Caravatti, G.; Floersheimer, A.; Furet, P.; Manley, P.; Vaupel, A.; Pissot Soldermann, C.; Gessier, F.; Schnell, C.; Littlewood-Evans, A. J.; Kapa, P. K.; Bajwa, J. S.; Jiang, X. Preparation of Bicyclic Amides as Kinase Inhibitors. PCT Int. Appl. WO 2006059234, 2006.

(21) Bold, G.; Vaupel, A.; Lang, M. Heterobicyclic Carboxamides as Protein Kinase Inhibitors and Their Preparation, Pharmaceutical

DOI: 10.1021/acs.jmedchem.5b01227
J. Med. Chem. 2015, 58, 9273−9286

Compositions and Use in the Treatment of Proliferative Diseases. PCT Int. Appl. WO 2008009487, 2008.
(22) Wan, Z.-K.; Wacharasindhu, S.; Levins, C. G.; Lin, M.; Tabei, K.; Mansour, T. S. The Scope and Mechanism of Phosphonium-Mediated S_NAr Reactions in Heterocyclic Amides and Ureas. *J. Org. Chem.* **2007**, *72* (26), 10194−10210.
(23) Ji, N.; Meredith, E. L.; Liu, D.; Adams, C. M.; Artman, G. D.; Jendza, K. C.; Ma, F.; Mainolfi, N.; Powers, J. J.; Zhang, C. Synthesis of 1-substituted-3-aminopyrazoles. *Tetrahedron Lett.* **2010**, *51*, 6799−6801.
(24) Johnson, L.; Powers, J.; Ma, M.; Jendza, K.; Wang, B.; Meredith, E. L.; Mainolfi, N. A Reliable Synthesis of 3-Amino-5-Alkyl and 5-Amino-3-Alkyl Isoxazoles. *Synthesis* **2013**, *45*, 171−173.
(25) (a) Jones, K. A.; Garbati, N.; Zhang, H.; Large, C. H. Automated patch clamping using the QPatch. *Methods Mol. Biol.* **2009**, *565*, 209−223. (b) Kutchinsky, J.; Friis, S.; Asmild, M.; Taboryski, R.; Pedersen, S.; Vestergaard, R. K.; Jacobsen, R. B.; Krzywkowski, K.; Schroder, R. L.; Ljungstrom, T.; Helix, N.; Sorensen, C. B.; Bech, M.; Willumsen, N. J. Characterization of potassium channel modulators with QPatch automated patch-clamp technology: system characteristics and performance. *Assay Drug Dev. Technol.* **2003**, *1*, 685−693.
(26) Zhou, L.; Yang, L.; Tilton, S.; Wang, J. Development of a High Throughput Equilibrium Solubility Assay Using Miniaturized Shake-Flask Method in Early Drug Discovery. *J. Pharm. Sci.* **2007**, *96*, 3052−3071.
(27) Takahashi, K.; Saishin, Yo.; Saishin; Yu; King, A. G.; Levin, R.; Campochiaro, P. A. Suppression and Regression of Choroidal Neovascularization by the Multitargeted Kinase Inhibitor Pazopanib. *Arch. Ophthalmol.* **2009**, *127*, 494−499.
(28) Connolly, T. J.; Matchett, M.; Sarma, K. Process Development and Scale-up of a Selective α_1-Adrenoreceptor Antagonist. *Org. Process Res. Dev.* **2005**, *9*, 80−87.
(29) Seelen, W.; Shäfer, M.; Ernst, A. Selective ring N-protection of aminopyrazoles. *Tetrahedron Lett.* **2003**, *44*, 4491−4493.

DOI: 10.1021/acs.jmedchem.5b01227
J. Med. Chem. 2015, 58, 9273−9286